Chapter 9

Isotope Ratio Control of K_2^+

This chapter describes a method to control the ionization ratio of the two potassium dimer isotopes $^{39,39}K_2^+$ vs. $^{39,41}K_2^+$ by employing shaped femtosecond laser pulses. The feedback loop is applied in order to selectively optimize the ratio of the two different isotopes in a three-photon ionization process, i.e. to maximize it or to minimize it, respectively.

Isotope selection is a steady growing topic in technology and science. History and paleontology, medicine and nuclear physics are only few of the fields in which the selectivity of different isotopes has gained a great interest. There are several methods which are widely used in order to separate particular isotopes.

Centrifugal isotope separation is a known applied method which uses a gas centrifuge machine. The gas consisting of different isotope molecules is rotated with a velocity of many hundreds of meters per second. The gas density radial distribution is determined by the centripetal acceleration. According to the Boltzmann formula, the gas density distribution depends on its molecular mass, thus one can select the desired isotope.

Other methods like deflection in electromagnetic fields, gaseous diffusion or ion cyclotron resonance heating in low-temperature plasma, take also advantage of the small mass difference [158].

Laser isotope separation of an atomic vapor is based on the small isotope shifts present in the absorption spectra. The atoms of the chosen isotope are selectively excited in a vaporized isotope mixture by a narrow-band laser radiation (e.g. a cw laser). The laser ionizes the atoms which are later collected. This process involves two steps of successive photo-excitation and photo-ionization. Laser isotope selection of molecular isotopes is based on the effect of isotopic selective multi-photon dissociation of molecules irradiated by infrared photons. The molecule absorbs radiation of a resonant infrared wavelength due to the interaction of its vibrating electric dipole with the

oscillating electric field of the laser. Its vibrational states are sequentially excited until the molecule fragments. Since the necessary wavelengths are determined by the masses of atoms constituting the molecule, the isotope selective excitation and dissociation can be separately performed.

Thus laser isotope separation techniques use the small shifts of vibrational levels of particular isotopes to achieve high-selectivity [159,160]. Nevertheless, a detailed knowledge of the system is essential. Isotope selective molecular dynamics by using femtosecond laser pulses were recently reported [53, 74]. Isotope separation by generating spatially localized wave packets due to the differences in their free temporal evolution was achieved as well [161].

The method employed in the following experiments takes advantage of the isotope shifts of the vibrational levels in the involved electronic excited states. In this way, a pronounced increase of one potassium dimer isotope compared to the other is achieved, e.g. by a factor of 141 [162]. From the acquired optimal pulse spectra one could obtain information about the optimally chosen excited states during the ionization path. Hence, a fingerprint of the molecular dynamics on the involved electronically excited states could be found in the optimal pulse shape. The applied method is demonstrated, as already mentioned, for the potassium dimer isotopes; nevertheless, selective isotope optimization should be valid, in general, for almost every isotopic molecule. First results on the heterogeneous alkali dimers $^{23}Na^{39}K$ and $^{23}Na^{41}K$ confirm the universality of the method [163, 164].

The introductory part of this chapter focuses on the choice of the investigated system; the next section contains the applied experimental method on selective optimization of the isotope ratio. A preliminary experiment in which two laser pulses were applied in a shaped–pump&probe scheme in order to increase/decrease the $^{39,39}K_2^+$/ $^{39,41}K_2^+$ ratio will be presented. Section 9.5 describes the isotope selective ionization in which a single shaped laser field was used. Thereby, either the phase or the amplitude of the input laser radiation (or both) were optimized in order to maximize/minimize the ratio. The results obtained are discussed in each section, whereby a comparison between phase and amplitude modulation and pure amplitude modulation with phase-only experiments is given in section 9.5.4. The experiments are performed also at different central laser wavelengths. The final section contains a summary followed by an outlook at possible future experiments.

9.1 Choice of the System

The natural abundance for the atomic potassium isotopes ^{39}K:^{40}K:^{41}K is 93.76:0.01:6.73 (in percentage), respectively. The isotope distribution of the

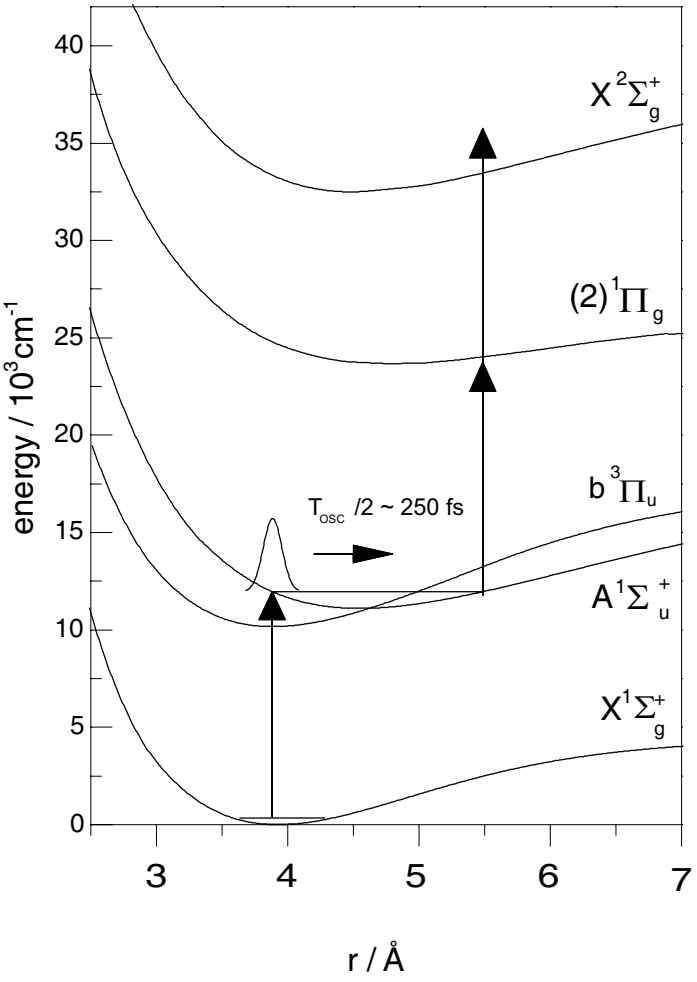

Figure 9.1: The potential energy surfaces involved in the multi-photon ionization for the $^{39,39}K_2$ dimer. The oscillation period of the wave packet on the $A^1\Sigma_u^+$ amounts $T_{osc} \sim 500$ fs.

potassium dimers in a molecular beam by multi-photon laser ionization was measured to be $^{39,39}K_2$:$^{39,41}K_2$:$^{41,41}K_2$ = 100:14.78:0.55 [165].

Alkali metal dimers are model systems of great interest in femtosecond pump–probe studies, since they can be easily ionized with commercially available Ti:sapphire oscillators. The potassium dimer has a pure 1 + 2-photon pump–probe transition mechanism [80]. In the past years the multi-photon ionization process of K_2 was investigated in our group [53] by means of femtosecond time-resolved spectroscopy. The experiments on the two species $^{39,39}K_2$ and $^{39,41}K_2$ are described in Chapter 5, section 5.1.5. A π phase shift appears between the oscillations of the two isotopes (see Figure 5.3). The

anti-phase behavior of the oscillations occurs first in the range between 5 and 15 ps.

It can be expected that the optimization algorithm would create an optimal pulse shape which maximizes or minimizes the isotope ratio[1] by taking advantage of this phenomenon. As it will be shown later in addition to the temporal behavior of the optimal pulse, its frequency pattern plays also an important role.

The main goal of the experiments presented in this chapter is not only to control the isotope ratio ionization on potassium dimers, but also to understand the underlying process by analyzing the acquired optimal pulse shapes. Since the optimal pulse shapes can be sometimes difficult to interpret, the attention is concentrated on simple model systems, e.g. dimers, where the number of possible (ionization) pathways is limited. Indications of half and integer values of the oscillation period within the optimized pulse shapes would give hints about the ionization path chosen by the molecule within the optimization experiment.

9.2 Experimental Preparations

The potassium dimers are produced in a molecular beam similar to the NaK dimers (see Chapter 8, section 8.2). Potassium metal of 99.5 % purity is usually purchased in sealed ampullae[2]. The ampullae are broken in a glovebox under Nitrogen atmosphere and the metal is inserted in one or two TZM skiffs of 4 to 6 cm length. The 2–3 grams of metal assured a continuous beam of at least 20 hours.

The oven containing the sample is then heated up to 450 °C. The potassium vapor co-expands with the carrier gas (Argon) through the 70–80 μm diameter nozzle into the vacuum. A 1 mm diameter skimmer is used to skim off the molecular beam after the supersonic expansion. The argon pressure is set to 1.3 bar, whereas the gas flow is about 20 standard cubic centimeters per minute. These stagnation conditions allow the production of K_2 dimers exclusively with no larger clusters present. Thus fragmentation of larger clusters into K_2 does not occur.

As femtosecond laser source the Spectra Physics Ti:sapphire oscillator (FS I) is used (80 MHz, 10 nJ, $\Delta\lambda \approx 8$ nm at FWHM). In the control experiments the laser wavelengths are tuned in the 810–833 nm spectral

[1]The ratio between the two isotopes should be understood as the ratio between the ion signal intensities measured by the secondary electron multiplier for the two isotopes, respectively. The notation $\Re = I(^{39,39}K_2^+)/I(^{39,41}K_2^+)$ used in this chapter refers to it.

[2]ABCR GmbH & Co. KG, Karlsruhe, Germany.

interval. The intensity of the focused laser beam it the interaction region with the cluster beam is estimated to be of the order of 1 GW cm^{-2} or less. Hence the experiments are done in the weak field limit. This will simplify the interpretation of the optimized process.

The laser pulses irradiate the neutral, cold molecules. The resulting ion signal is extracted by the quadrupole mass spectrometer and detected by a secondary electron multiplier.

9.3 Acquisition of the Experimental Data

The irradiated dimers are extracted by a quadrupole mass spectrometer (QMS). The QMS allows the detection of 16 different masses on 16 channels, respectively. For the measurements described in this chapter, a routine to perform the selection of the two potassium dimer isotopes was developed.

Figure 9.2 shows the principle of the data acquisition. Through its analog port, the QMS displays the ion signal of the two isotopes on two different channels. The recorded signal is digitalized by the SR 245 Analog/Digital (A/D) converter. A trigger signal is provided in order to separate the two ion signals. The trigger signal is measured on the second channel.

The QMS requires a certain time delay to switch between the channels (masses). This has an influence on the simultaneous monitorization of the two masses. The A/D converter measures the analog output voltage continuously. Hence the data recorded during the switch time has to be removed. Figure 9.2d presents an algorithm used to eliminate the data measured during the switch time and to allow the correct measurement of the two isotopes by using the trigger level.

The evaluation of each individual begins at a random time. The software (see Ref. [40]) has to ensure that there are enough data points (e.g. 15 points) measured for each isotope. The recorded data (number of points) is later on averaged. The sampling is though limited by the readout frequency (100 Hz) of the A/D converter.

The evolutionary algorithm assigns the measured signal given the starting point and the trigger level. When the trigger level changes and 15 points of the ion signal of one isotope were collected, the routine records 15 other values of the second isotope. When the routine has not measured the 15 needed points, after the trigger signal is switched, it stops measuring and ”waits” for the time corresponding to 3 or 4 data points in order to exclude these values. Then it continues collecting data points for the second isotope. When the trigger level changes again, the routine ”waits” again 3–4 data points to ”pass” and thereafter records the remaining data for the first isotope.

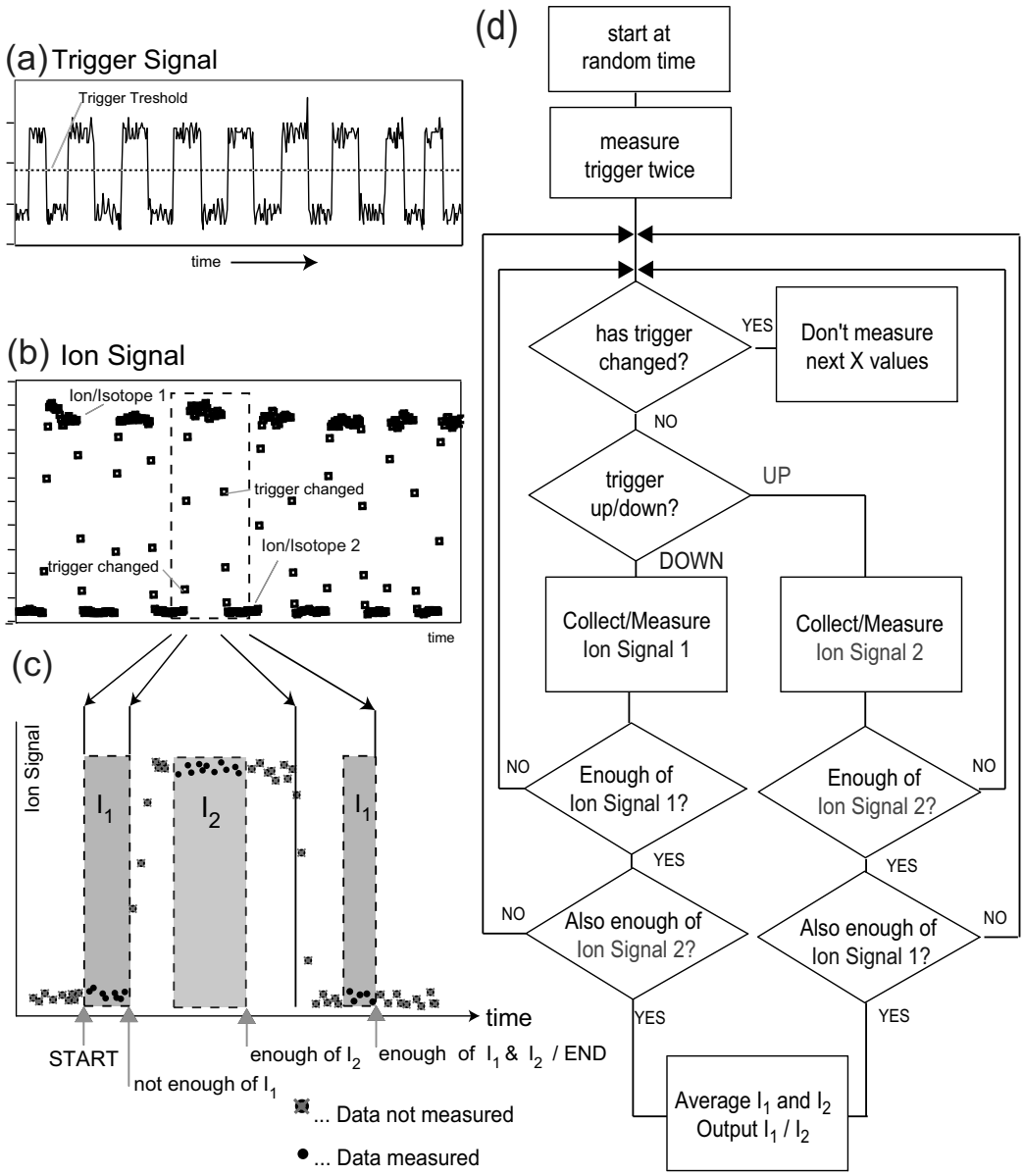

Figure 9.2: Scheme of the acquisition of the experimental data in the isotope ratio control experiments. The two masses are measured on two separate channels of the quadrupole mass spectrometer (taken from [40]).

The two ion signals are averaged when enough data is acquired (15 points for each isotope) and the ratio $\Re$ is calculated. The ratio $\Re$ represents the fitness function for the evolutionary algorithm and depending on the task, it can be maximized or minimized.

The ratio of the averaged value of the 15 collected data points for each isotope represents a single individuum in the evolutionary algorithm. The computer needs usually ca. one second to calculate the ratio (one individuum). In the first generation, the evolutionary algorithm starts with a random population of 10 individuals (10 arbitrary pulse forms). After their recombination, 30 individuals are created and sent to the mutation operator. If the case of mutation success (the $\frac{1}{5}$ rule of success), the ratio $\Re$ is multiplied by 1.3. Otherwise the ratio is multiplied by 0.8. The *survival of the fittest* operator selects the 10 out of 30 individuals which have produced the highest (or lowest in the case of minimization) ion signal ratio $\Re$.

Due to the readout time delay of the A/D converter, switch time of the QMS, the time the computer needs to calculate, the time the liquid crystals in the modulator need to rotate, the feedback algorithm requires about 20 seconds/generation. This corresponds to a time duration of at least 60 minutes for one complete experiment.

9.4 Two-Pulse Optimization of the $^{39,39}K_2^+/^{39,41}K_2^+$ Ratio

In this section the experiment performed with a shaped-pump&probe scheme is described. The output femtosecond laser beam from the Ti:sapphire oscillator (see FS I, Chapter 4 section 4.2.1) is split in two parts by an optical beamsplitter. One beam is sent through the pulse shaping apparatus (shaped pump), whereas the second beam passes the computer-controlled optical delay stage (probe). The two beams are recombined in a second beamsplitter as in a Mach-Zhender interferometer.

The excitation process performed by the shaped-pump pulse is iteratively optimized by the self-learning algorithm. The probe pulse is sent "at the right time", e.g. when there is a π phase shift between the oscillations of the two isotopes. The goal of the evolutionary algorithm is to find a laser pulse which maximizes or minimizes the ratio $\Re$ of the two potassium dimer isotopes.

Figure 9.3 reproduces the pump–probe experiments on the two K_2 isotopes from Ref. [53]. The beat structure in the $^{39,39}K_2$ spectrum and the dephasing in the $^{39,41}K_2$ transient are present. These features are discussed in section 5.1.5. The recurrence in the $^{39,41}K_2$ isotope kinetic trace starts around 5 ps. The π phase shift between the oscillations of each species with respect to the other is present until 15 ps. Hereafter another π phase shift occurs and the oscillations of the two isotopes are in phase again. The first attempt was to send the probe pulse at 9 ps. At this time delay one expects

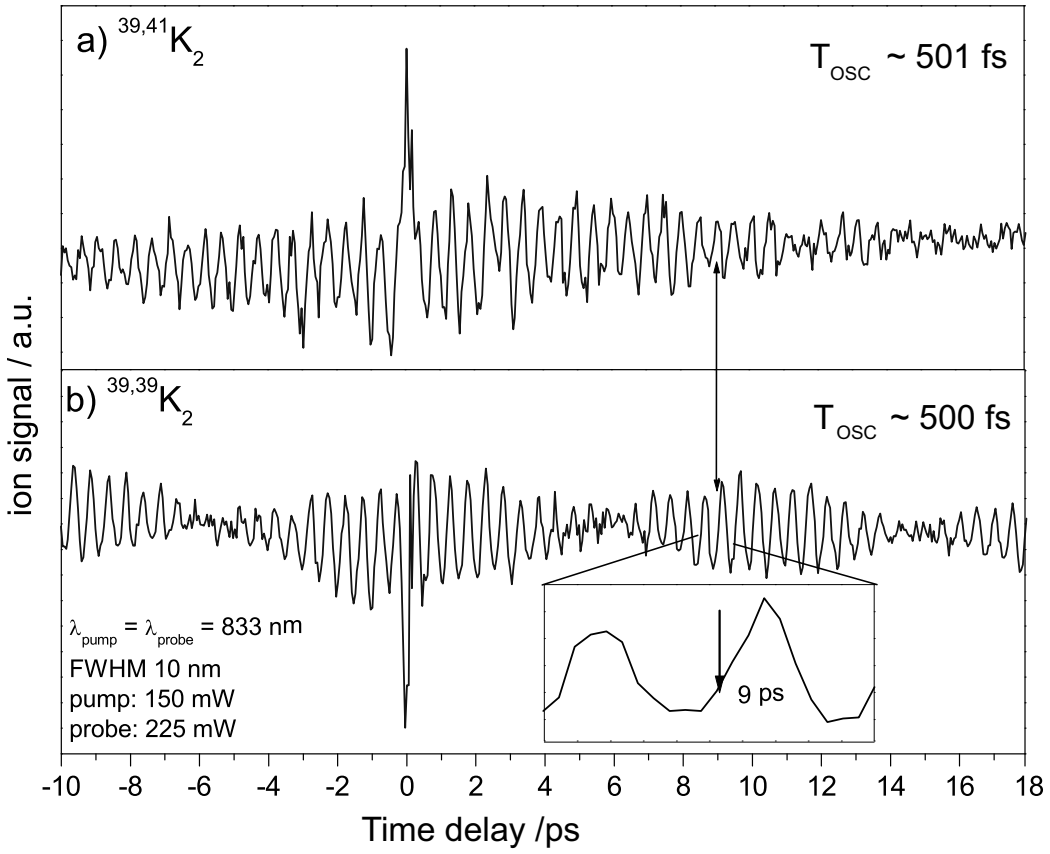

Figure 9.3: Time resolved spectra recorded for both isotopes $^{39,41}K_2$(a) and $^{39,39}K_2$ (b) which reproduce the results from Ref. [53]. The beating structure for $^{39,39}K_2$ with a period of $T_{beat} \approx 10$ ps and the wave packet dephasing for $^{39,41}K_2$ are visible. At 9 ps, when the probe pulse is sent, the control experiment described in this section tries to find an optimal laser field which optimizes the excitation step.

a successful isotope ratio control since the isotope-dependent dynamics are very well separated [76].

The average laser power of the employed shaped-pump and probe pulses amounted 150 mW and 225 mW, respectively. The two pulses were centered around 833 nm and their spectral bandwidth is about 10 nm at FWHM.

From the pump–probe traces in Figure 9.3 one obtains a ratio of the two isotopes of 1.25 for the maximization and 0.8 for the minimization. The maximization factor of 1.25 is obtained by dividing the value at the maximum of the oscillation's amplitude of $^{39,39}K_2$ with its time-corresponding value of the amplitude in the minimum of the $^{39,41}K_2$ spectrum. The minimization factor of 0.8 is calculated by dividing the minimum of an amplitude value

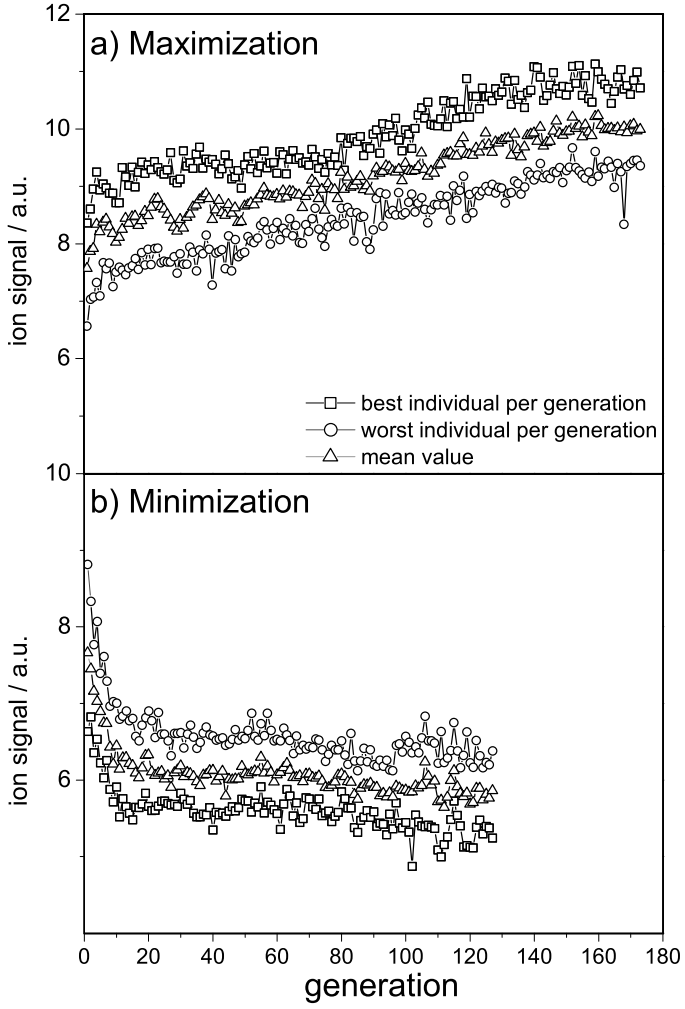

Figure 9.4: Progression of the ratio $\Re$ =I($^{39,39}K_2$)/I($^{39,41}K_2$) of the two isotopes during two-pulse optimization for maximization (a) and minimization (b). The squares represent the best individual per generation, the circles show the worst individual per iteration and the triangles their mean value. The normal isotope ratio in the molecular beam is $\Re_n = 6.9$. The ion ratio $\Re$ is modified by a factor of $\Re_{max} = 1.4$ for the maximization and by a factor of $\Re_{min} = 0.74$ for the minimization, leading to an overall alteration of the isotope ratio of $\Re_{max}/\Re_{min} = 1.9$.

of the $^{39,39}K_2$ oscillation with its time-correspondent amplitude's maximum value of the $^{39,41}K_2$ isotope oscillations. Thus the variation of the isotope ratio in the pump–probe spectra is almost 1.6.

Figure 9.4 shows the evolution of the ion signal ratio $\Re$ during the optimization procedure performed with the shaped-pump&probe scheme for

	Frequency / cm^{-1}			
Transition	**Maximization**	Theory	**Minimization**	Theory
$v_A' = 12 \leftarrow 0$	11917	11919	11899	11908
$v_A' = 13 \leftarrow 0$	11980	11986	11973	11974
$v_A' = 14 \leftarrow 0$	12045	12051	12028	12038
$v_A' = 15 \leftarrow 0$	12114	12117	12099	12104
$v_\pi' = 5 \leftarrow 12$	12008	12007	—	—
$v_\pi' = 7 \leftarrow 14$	—	—	11997	11993

Table 9.1: Some of the frequencies observed in the optimal pulse spectra (Figure 9.5) for isotope ratio optimization of the potassium dimers correspond to transitions between vibrational levels of the electronic states $A^1\Sigma_u^+ \leftarrow X^1\Sigma_g^+$ and $2^1\Pi_g \leftarrow A^1\Sigma_u^+$. The theoretical values are taken from Ref. [81].

both maximization and minimization. In the case of maximizing the ratio an optimization factor of $\Re_{max} = 1.4$ is achieved. After the minimization experiment the ion signal ratio was reduced by a factor of $\Re_{min} = 0.74$. The factors are calculated with respect to the regular isotope ratio in the supersonic jet under the given experimental conditions of $\Re_n = 6.9$. Thus the variation of the isotope ratio signal between maximization and minimization is $\Re_{max}/\Re_{min} = 1.9$, which is higher than expected from the pump–probe measurements. Hence there are other effects responsible than an optimal excitation followed by an ionization step.

Recording the optimal pulses would allow one to get an insight in the optimized process. The laser pulse spectra for both maximization and minimization of the ratio $\Re$ are shown in Figure 9.5a and Figure 9.5b, respectively. The two spectra exhibit sharp peaks with different alternating intensities. Between consecutive peaks the intensity measured by the spectrometer is not attenuated to zero. The sharp peaks in the minimization experiment are located at different frequencies compared to the maximization case. They are shifted in average by ~ 12 cm^{-1}. This number corresponds to the calculated value of the isotopic shift, which is predominantly present in the excited state between the two isotopes of the potassium dimer [81]. Table 9.1 summarizes the frequencies allocated to the involved transitions between the vibrational levels of the electronic states $A^1\Sigma_u^+ \leftarrow X^1\Sigma_g^+$, and $2^1\Pi_g \leftarrow A^1\Sigma_u^+$.

Several peaks in the spectra (see also Table 9.1) can be assigned to transitions to estimated vibrational levels is the $2^1\Pi_g$ state. This was calculated by solving the time-independent Schrödinger equation numerically for the potential curve [80, 166]. Both isotopes are excited by the pump pulse from

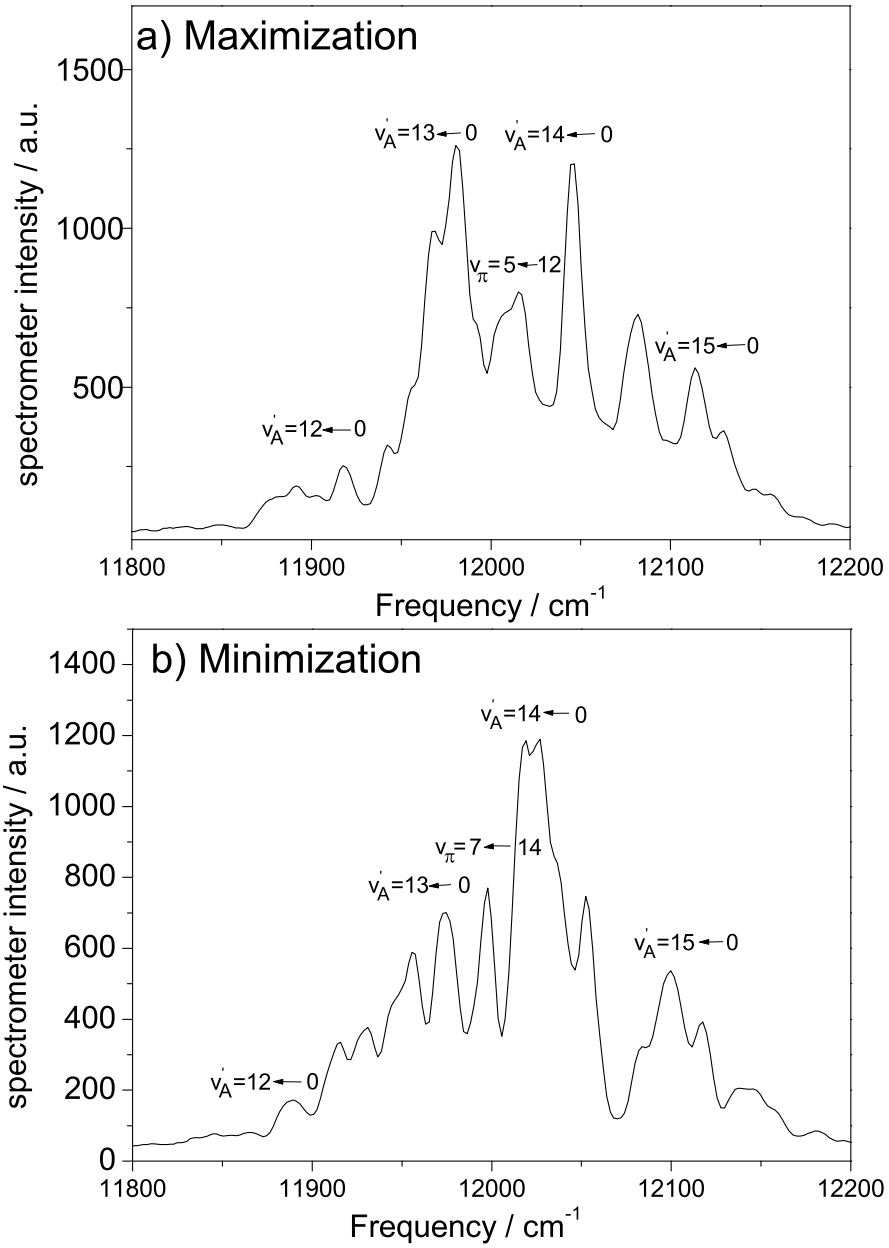

Figure 9.5: Spectra of the optimal pulses obtained for maximization (a) and minimization (b) of the ratio $\Re$ by employing the two-pulse optimization scheme. A few of the sharp peaks can be associated with the transitions between the vibrational levels of the different electronic states $A^1\Sigma_u^+ \leftarrow X^1\Sigma_g^+$ and $2^1\Pi_g \leftarrow A^1\Sigma_u^+$ of the $^{39,39}K_2$ isotope (a) and of the $^{39,41}K_2$ isotope (b). The peaks for minimization are shifted on average by 12 cm^{-1} with respect to the corresponding peaks for maximization. The transmission pixel pattern of the modulator corresponds to the peaks in the optimal pulse spectra.

$v_X = 0$ in the electronic ground state $X^1\Sigma_g^+$ to the $v_A^{'} = 12, 13, 14, 15$ in the excited state $A^1\Sigma_u^+$. Further separation of the potassium dimers takes place in the next excitation step, whereby for maximization the transition $v_\pi^{'} = 5 \leftarrow 12$ to the second resonant excited state $2^1\Pi_g^+$ occurs. Apparently for minimization another transition between vibrational levels of the two electronic excited states is involved: $v_\pi^{'} = 7 \leftarrow 14$.

Thus the pump pulse transfers the population from the ground state $X^1\Sigma_g^+$ to the excited $A^1\Sigma_u^+$ state for both isotopes, as indicated in the spectra from Figure 9.5. Since in the optimal pulse (shaped–pump pulse) an indication of transitions between the $A^1\Sigma_u^+$ and $2^1\Pi_g$ states is found, it can be concluded that the pump pulse transfers population from the $A^1\Sigma_u^+$ to the ion state via the intermediate $2^1\Pi_g$ state as well. Nine picoseconds later the probe pulse ionizes the molecules predominantly from the $A^1\Sigma_u^+$ state, but it can transfer population to the ion state from the $2^1\Pi_g$ state as well. The appearance of the transition $2^1\Pi_g \leftarrow A^1\Sigma_u^+$ is an unexpected result since the shaped-pump pulse was chosen to optimize only the first excitation step, whereas the role of the probe pulse was expected to ionize the system after 9 ps, resonantly from the $A^1\Sigma_u^+$ state via the $2^1\Pi_g^+$ state.

The cross-correlations of the optimal pulses obtained for maximizing and minimizing the ratio $\Re$ are depicted in Figure 9.6. The figure contains also the XFROGs of the corresponding optimal pulses as well.

The cross-correlation traces of the optimal pulse shapes are recorded with a short pulse directly from the laser. They exhibit pronounced structures for both maximization (Figure 9.6a) and minimization (Figure 9.6b). Multiples of the half-period of oscillation can be observed between some intensity maxima, but an accurate explanation of the temporal behavior of the two isotopes can not be given at this point.

The XFROG traces obtained for maximization and minimization of the ratio $\Re$ are shown in Figures 9.6c and 9.6d, respectively. The XFROGs represent a convolution of the short reference pulse with the shaped test pulse. This leads to a smoothing of the frequency components due to the broad bandwidth (10 nm) of the reference spectrum. The result hinders the observation of the sharp peaks present in Figure 9.5. Information about the chirps can not be read out, but some general aspects can be outlined. The wavelength shift of approximately 1 nm between two adjacent pulses in the case of maximization (Figure 9.6c) could suggest a consecutive excitation of the vibrational levels in the involved electronic states on the selected optimal ionization pathway.

The factors obtained in the optimization experiment, higher than in the pump–probe spectra, demonstrate the capability of the feedback-loop approach to iteratively develop a shaped laser pulse which modifies the isotope

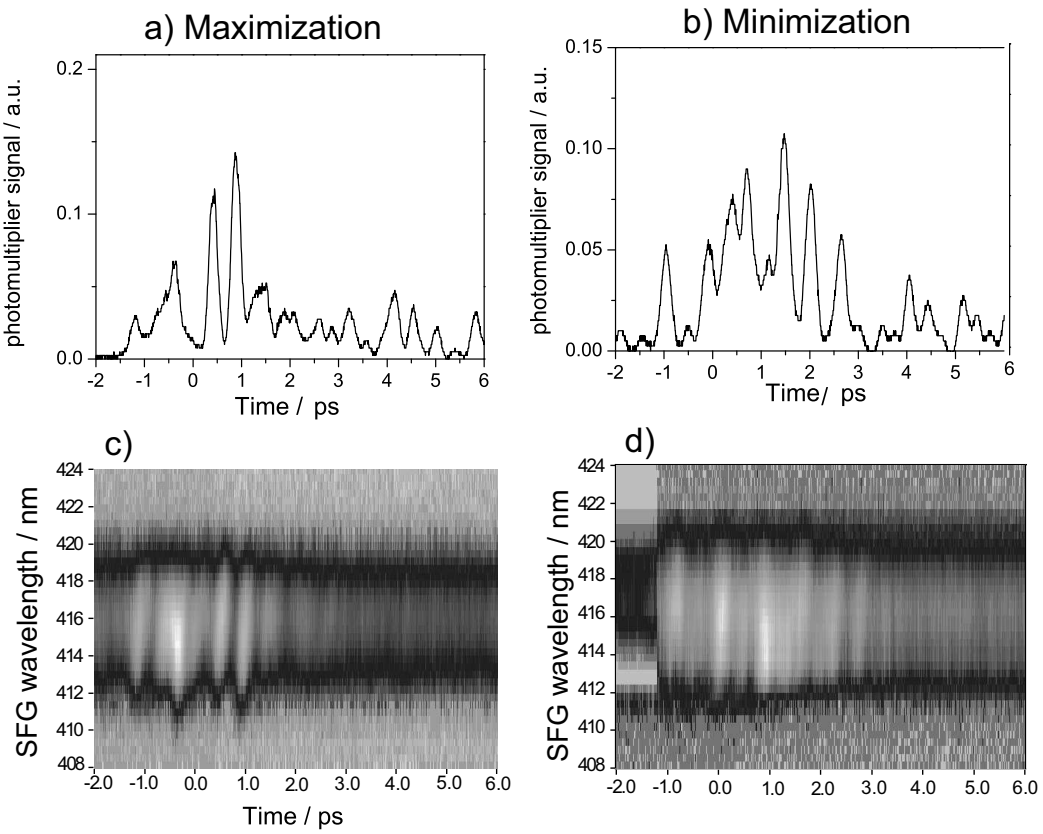

Figure 9.6: Cross-correlation and the corresponding XFROG traces of the optimal pulses obtained for maximization (a) and minimization (c) of the ratio $\Re$ by employing the shaped-pump&probe scheme. The two traces feature a complex series of several subpulses over approximately 7 ps for both maximization (a) and minimization (b). The two pulses were centered around 833 nm.

ratio rather than a short pulse. Considering that the experimental conditions were chosen to ensure an optimal isotope selection by wave packet separation, apparently there are other phenomena responsible for isotope selection than wave packet recurrences. Since the evolutionary algorithm does not have the freedom to considerably change the isotope ion ratio $\Re$, due to the presence of the second short pulse (probe) which always irradiates the two isotopes, a single-shaped pulse optimization experiment is necessary. In this way each single-shaped pulse performs the entire three-step ionization process. The single-pulse would allow a larger feasibility of the feedback-loop optimization procedure to be used in its full extent.

9.5 Single-Pulse Optimization of the $^{39,39}K_2^+/^{39,41}K_2^+$ Ratio

This section treats the isotope selection experiments at different wavelengths, whereby either the phase and/or the amplitude of the single-shaped pulse is optimized in an iterative process. The laser field passes through the pulse shaping apparatus and irradiates the potassium dimers. Their ratio $\Re$ is measured as described in section 9.3.

First the optimization experiments at 833 nm central wavelength are presented. Here both the phase and the amplitude of the laser field are optimized. The next subsection describes the control experiments in which only the phase of the laser field is iteratively changed at the same central wavelength. Amplitude-only optimization experiments performed at 833 nm are presented as well. A comparison between the experiments at 833 nm tries to analyze which of the frequency and temporal patterns in the optimal pulses is more significant. Further phase and amplitude optimization experiments at different central wavelengths, 820 nm and 810 nm, are reported in the final two sections. The conclusions are summarized at the end of the chapter and an outlook is given.

9.5.1 Phase and Amplitude Modulation at 833 nm

By using a single shaped pulse which performs the entire ionization process, one does not expect wave packet dephasing phenomena to contribute to the optimized process because of the limited modulation time window of the pulse shaper. The SLM-256 mask can generate pulse trains separated in time by a maximum of 5 ps.

The short, non-optimized laser pulse is centered around 833 nm, its bandwidth amounts $\Delta\lambda = 7$ nm and the average power is 320 mW. After ion ratio maximization the power is $P_{max} = 120$ mW, whereas after ion ratio minimization, the laser power is $P_{min} = 60$ mW. The difference between the input and output power is due to amplitude modulation effects.

Figure 9.7 shows the progression of the isotope ion ratio $\Re$ during the optimization of both phase and amplitude of the single laser field. The two optimization experiments of maximization (Figure 9.7a) and minimization (Figure 9.7b) start from the regular isotope ratio value of $\Re_n = 6.9$. In the case of maximization, a modification of the isotope ratio to $\Re_{max} = 72$ is observed. In the minimization experiment the ion ratio monotonously decreases below 1. Hereby the isotope ion ratio is reversed to $\Re_{min} = 0.51$. It is important to mention that the values given for the factors are referred to

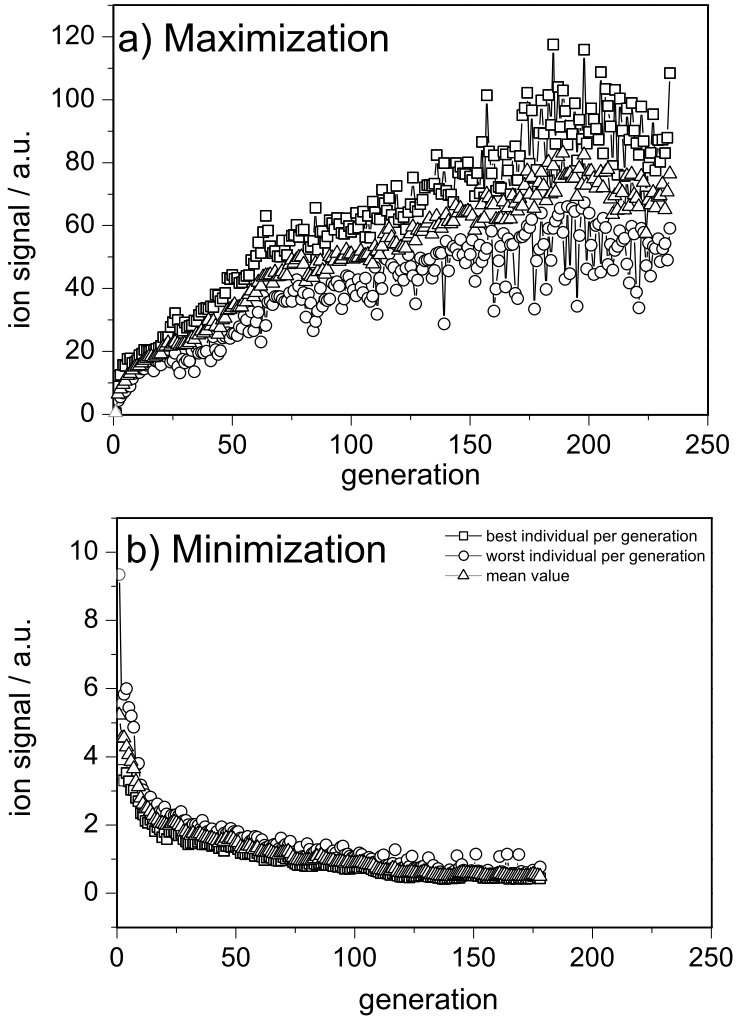

Figure 9.7: Evolution of the ion signal ratio $\Re$ =I($^{39,39}K_2$)/I($^{39,41}K_2$) during single pulse optimization (both phase and amplitude). (a) Evolution during ratio maximization, whereby a ratio $\Re_{max} = 72$ was achieved. (b) Evolution during ratio minimization, whereby the ratio $\Re_{min} = 0.51$ is obtained. The isotope ratio $\Re$ is modified by a factor of 141 (see also the mass spectra in Figure 9.8). The squares represent the evolution of the best individual within a generation, the circles the evolution of the worst individual and the triangles their mean value.

the mean value of the best individuals.

This can be seen also in the mass spectra depicted in Figure 9.8 or by monitoring the ion signal produced by the short pulse, the optimal pulse for maximization and the optimal pulse for minimization. The alteration of the isotope ratio corresponds to a factor of $\Re_{max}/\Re_{min} = 141$. This is sur-

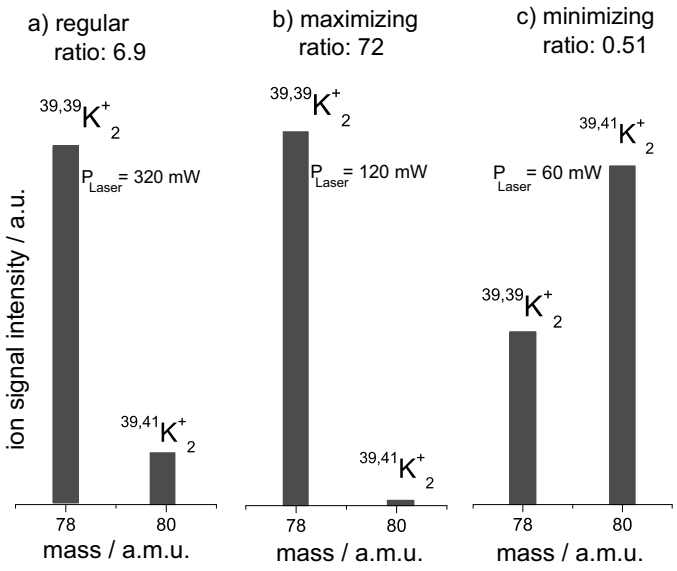

Figure 9.8: Mass spectra of the potassium dimer molecular beam recorded by laser multi-photon ionization with pulses centered at 833 nm before optimization (a), after the maximization of the ion ratio (b) and after the minimization of the ion ratio (c). Hereby both the phase and amplitude of the laser pulse are modulated. The average laser power before the experiment (a), after ratio maximization (b) and ratio minimization (c) is given as well.

prisingly high, compared to the results obtained by employing the shaped-pump&probe scheme (section 9.4) were the experiment conditions were chosen to assure an optimal wave packet separation.

The effect of the phase and amplitude modulation is very pronounced in comparison to the phase-only optimizations and amplitude-only modulation experiments, described in sections 9.5.2 and 9.5.3.

The spectra of the optimal pulses obtained for maximization and minimization are shown in Figure 9.9a and Figure 9.9b, respectively. Sharp peaks with different intensities are distinguishable. For maximization the peaks are situated at different frequencies compared to the peaks for minimization. They are shifted by ~ 12 cm^{-1}. Between the peaks, the intensity measured by the optical fiber spectrometer decreases in some cases to almost zero. Some of the peaks can be identified with transitions between different vibrational energy levels of the electronic excited states present in the optimized process. In the case of minimization the peaks are located at positions where the intensity in the maximization is low. Similarly, where the spectral intensity is high in the optimal spectrum obtained for maximization, there is almost

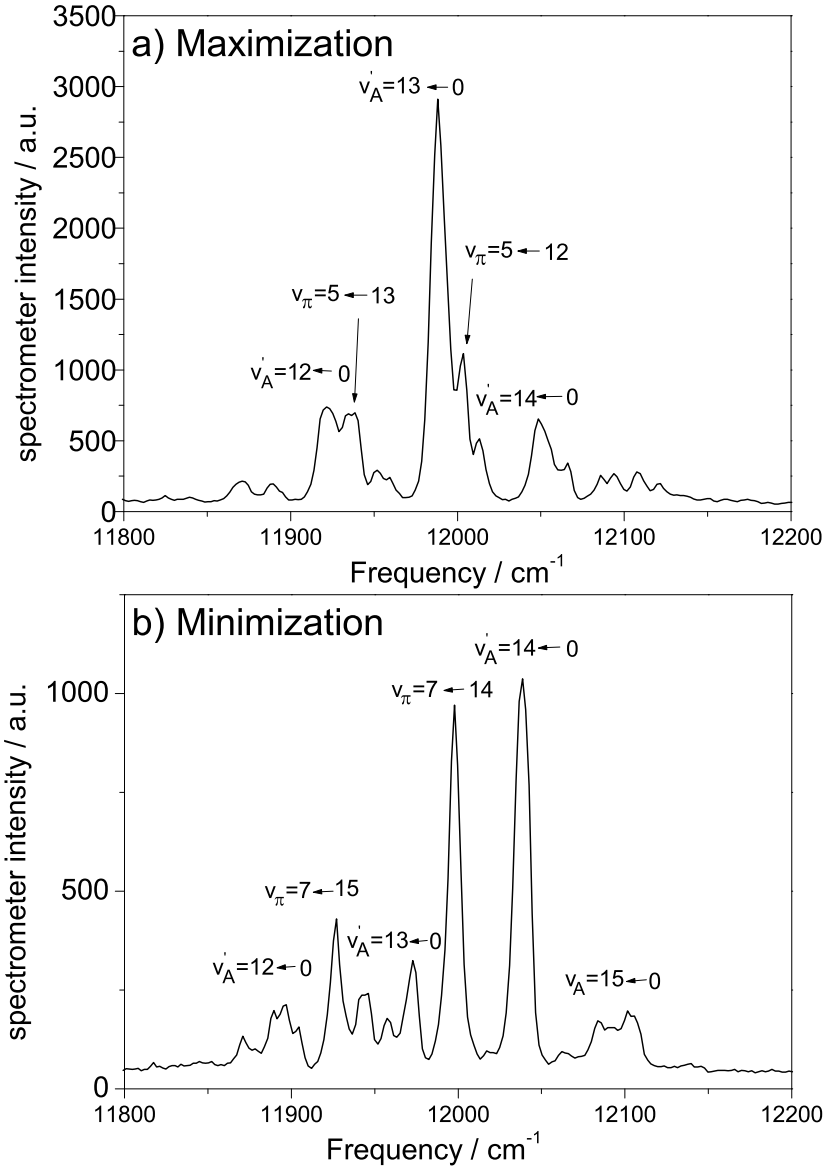

Figure 9.9: Spectra of the optimal pulses obtained for maximization (a) and minimization (b) of the ratio $\Re$ by employing the single pulse optimization procedure. The sharp peaks reveal the transitions between the involved vibrational levels of the different electronic states $X^1\Sigma_g^+$, $A^1\Sigma_u^+$, and $2^1\Pi_g$ of the $^{39,39}K_2$ isotope (a) and of the $^{39,41}K_2$ isotope (b). The transmission pixel pattern of the modulator corresponds to the observed peaks in the spectra of the optimized pulses, respectively. Both phase and amplitude of the laser field were optimized. The central wavelength was 833 nm.

	Frequency / cm^{-1}			
Transition	**Maximization**	Theory	**Minimization**	Theory
$v_A^{'} = 12 \leftarrow 0$	11921	11919	11899	11908
$v_A^{'} = 13 \leftarrow 0$	11987	11986	11974	11974
$v_A^{'} = 14 \leftarrow 0$	12049	12051	12038	12038
$v_A^{'} = 15 \leftarrow 0$	—	—	12100	12104
$v_\pi^{'} = 5 \leftarrow 12$	12003	12007	—	—
$v_\pi^{'} = 5 \leftarrow 13$	11936	11938	—	—
$v_\pi^{'} = 7 \leftarrow 14$	—	—	11997	11994
$v_\pi^{'} = 7 \leftarrow 15$	—	—	11926	11929

Table 9.2: The identified frequencies observed in the optimal pulse spectra in Figure 9.9 for ion ratio optimization of the two K_2 isotopes for both maximization and minimization. The frequencies correspond to transitions between the indicated vibrational levels of the $X^1\Sigma_g^+$, $A^1\Sigma_u^+$, and $2^1\Pi_g$ electronic excites states. The theoretical values are taken from Ref. [81].

no intensity in the pulse spectrum recorded for the minimization case. This certainly accounts for high isotope selectivity.

An indication of the distortion of the $v_A' = 13$ vibrational level in the $A^1\Sigma_u^+$ excited state might be observed as a small peak shift in the spectra for the maximization and minimization. As the LC modulator operates in this case at its resolution limit, the distortion of the aforementioned vibrational level due to spin-orbit effects can not be exactly assigned.

Table 9.2 contains the quantitative data from the optimal pulse spectra obtained in both maximization and minimization. The identified frequencies correspond to the transitions between particular vibrational levels of the involved electronic excites states $X^1\Sigma_g^+$, $A^1\Sigma_u^+$, and $2^1\Pi_g$ [81].

The slight differences in the assignment of frequencies of a few cm^{-1} are within the experimental error. The number of possible transitions identified is less than in the shaped-pump&probe case. This is understood by the fact that the input laser spectrum is less broad ($\Delta\lambda = 7$ nm) than the laser spectrum in the two-pulse optimization experiment ($\Delta\lambda = 10$ nm).

Some of the peaks in the optimal pulse spectra in Figure 9.9 are assigned to transitions to estimated vibrational levels in the $2^1\Pi_g$ state. The calculations were done by solving numerically the time-independent Schrödinger equation for the $^{39,39}K_2$ dimer in Ref. [80]. These levels show isotope shifts as well and may contribute to the high isotope selectivity. This demonstrates the capability of the presented isotope ratio control method, since it is not restricted to a single transition. The population is transferred from the elec-

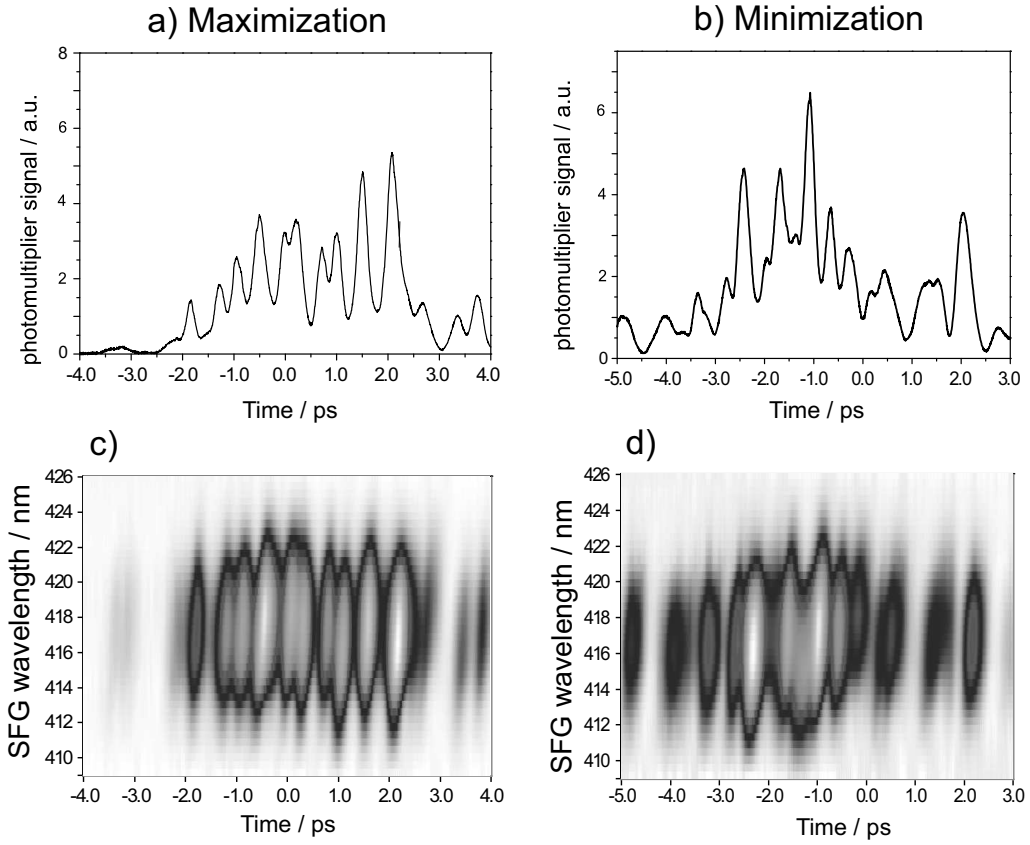

Figure 9.10: Cross-correlation and XFROG traces of the optimal pulses obtained for maximization and minimization of the ratio $\Re$ by employing single-pulse optimization scheme at a central wavelength of 833 nm. Both cross-correlation traces for maximization (a) and minimization (c) exhibit a complex series of pronounced intensity maxima spread over ~ 6 ps. The XFROG traces for maximization (b) and minimization (d) are shown as well.

tronic ground state $X^1\Sigma_g^+$ to the $v'_A = 12, 13, 14$ vibrational levels in the electronic excited state $A^1\Sigma_u^+$. From here transitions to other vibrational levels in the electronic state $2^1\Pi_g$ ($v_\pi^{'} = 5 \leftarrow 12, 13$ for maximization and $v_\pi^{'} = 7 \leftarrow 14, 15$ for minimization, respectively) occur during the multi-photon ionization process.

The cross-correlation of the optimal pulses obtained for maximization and minimization are presented in Figure 9.10a and Figure 9.10b, respectively. The corresponding XFROG spectrograms are shown in Figure 9.10c Figure 9.10d, respectively. One would expect to see the spectral features from Figure 9.9 in the projection on the wavelength axis of each corresponding

XFROG measurement. However it is known that a XFROG trace is recorded as a convolution of the short reference pulse with the shaped test pulse. The smoothing of the spectral components due to the relatively broad bandwidth (Δt = 7 nm at FWHM) of the reference spectrum makes these features indistinguishable.

In the present study an accurate explanation of the cross-correlation measurements and the XFROG traces cannot be given. Nevertheless, some general statements can be made. The complex pulse shapes contain a series of subpulses which are frequently separated by 250 fs. This corresponds to half the observed oscillation period of T_{osc} = 500 fs for the potassium dimers in the $A^1\Sigma_u^+$ state (see section 9.1). This can be understood as a stepwise excitation process: excitation at the inner turning point of the $A^1\Sigma_u^+$ state, followed after 250 fs by an excitation at the outer turning point. This is indeed supported by the known fact that at the outer turning point the Franck-Condon window is open to a resonant transition to the $2^1\Pi_g$ state (see Figure 9.1 and Refs. [53, 80]). Figure 9.9 also suggests that in the case of minimization, the excitation step $A^1\Sigma_u^+ \leftarrow X^1\Sigma_g^+$ takes place at other frequencies than the transition $2^1\Pi_g \leftarrow A^1\Sigma_u^+$. The up to 1 nm difference in the central wavelength observed between a few subpulses in the XFROG trace for minimization (Figure 9.10d) can be also responsible for a stepwise excitation process, leading to an enhanced optimization factor.

One can also take into account that isotope dependent constructive and destructive interferences between the propagating wave packets may occur within the ionization pathway as well. Their contribution would produce intensity maxima and minima within the temporal shape of the optimal pulse and would enhance the isotope specific ionization phenomenon (see also section 9.5.2).

Oscillations of wave packets generated on other electronic excited states than the one observed in the pump–probe analysis could also contribute to the complex form of the optimal pulses.

9.5.2 Phase Modulation at 833 nm

In order to better understand the isotope ratio control mechanism performed at 833 nm central wavelength and described in the previous section, the combination of phase and amplitude modulation is separated into phase-only and amplitude-only optimizations of the laser field. The phase-only modulation is reported throughout the present section and the amplitude-only experiments are described in section 9.5.3. Phase-only experiments would give hints on the relevance of the chirps and the temporal duration of the optimal pulses in the selective multi-photon ionization process.

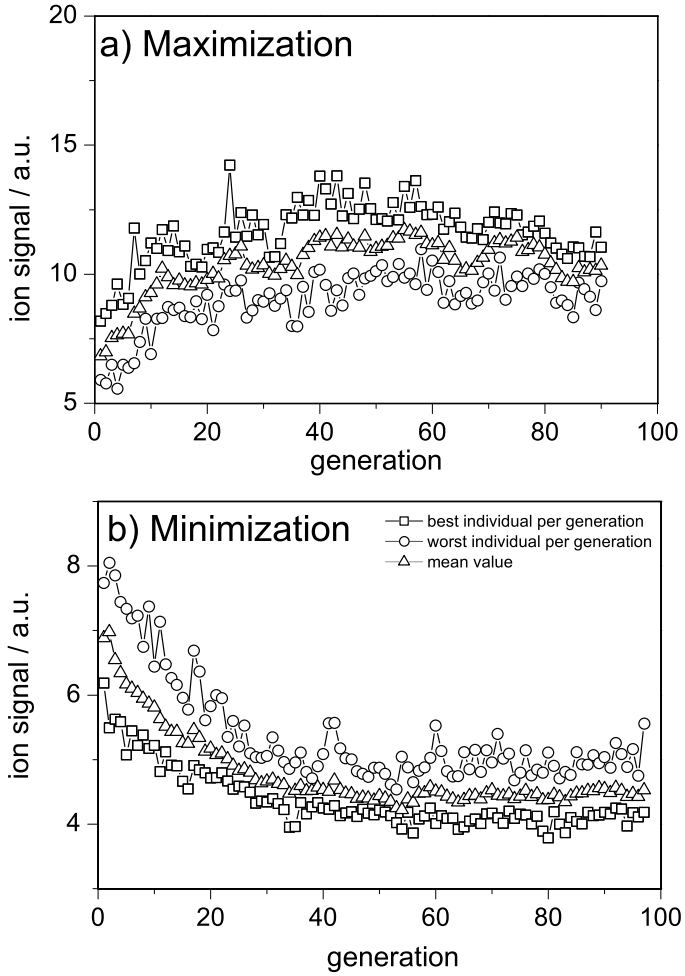

Figure 9.11: Progression of the ion signal ratio $\Re$ =I($^{39,39}K_2$)/I($^{39,41}K_2$) during phase only optimization. (a) Progression during ratio maximization, whereby a ratio $\Re_{max} = 11$ was achieved. (b) Evolution during ratio minimization, whereby the ratio $\Re_{min} = 4.3$ is obtained. The isotope ratio $\Re$ is modified by a factor of $\Re_{max}/\Re_{min} = 2.5$ (see also the mass spectra in Figure 9.12). The squares represent the evolution of the best individual within a generation, the circles the evolution of the worst individual and the triangles their mean value.

In Figure 9.11 the curves indicating the evolution of the ion signal ratio $\Re$ for each generation are presented. Both curves show the best, the mean and the worst of all values in one generation. In the case of maximization (Figure 9.11a) accidental fluctuations in the molecular beam were present. The noise in the present experiment is measured to be ±4–5 %. This can cause the best individual in one generation to produce a lower ion signal

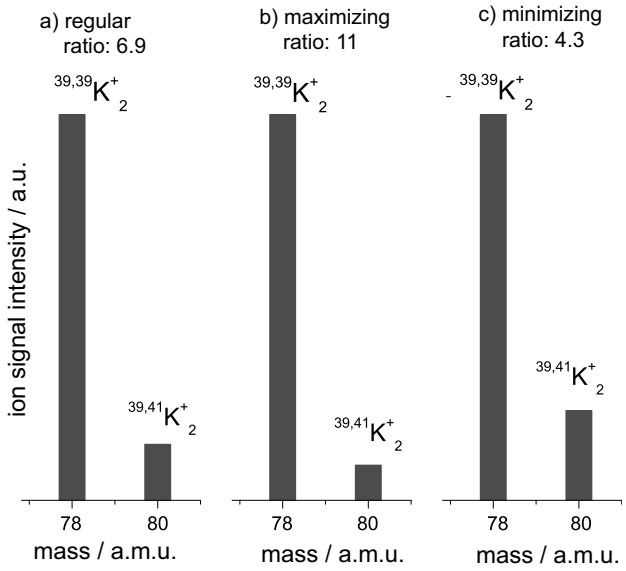

Figure 9.12: Mass spectra of the potassium dimer molecular beam recorded by laser multi-photon ionization for phase-only modulation experiments. (a) Mass spectrum measured with a short pulse before optimization. (b) Mass spectrum recorded with the optimal pulse obtained for maximization. (c) Mass spectrum taken with the optimal pulse for minimization.

ratio (small negative variations) in the next generation. If additionally all other individuals produce less ion ratio yield than the previous best one, a decrease of the ion signal ratio in the evolution of the best individual can occur. The ion signal ratio $\Re$ obtained for maximization is measured to be $\Re_{max} = 11$, compared to the regular ratio of $\Re_n = 6.9$. Thus the maximization factor is $\Re_{max}/\Re_n = 1.6$.

The minimization experiment in which only the phase of the laser pulse is modified leads to a regression of the ion signal ratio to $\Re_{min} = 4.3$, indicating a minimization factor of $\Re_{min}/\Re_n = 0.62$. The factors are calculated by taking the mean values into account.

Thus the isotope ratio $\Re$ is modified by a factor of $\Re_{max}/\Re_{min}= 2.5$. Compared to the variation of $\Re$ for phase and amplitude modulation of about 141 (see section 9.5.1) the total isotope ratio variation is very low. Nevertheless a higher factor than the isotope ratio in the pump–probe experiments is obtained.

Figure 9.12 shows the mass spectra of the molecular beam of potassium dimers recorded by laser multi-photon ionization with a short pulse (Figure 9.12a), the optimal pulse for ratio maximization (Figure 9.12b) and

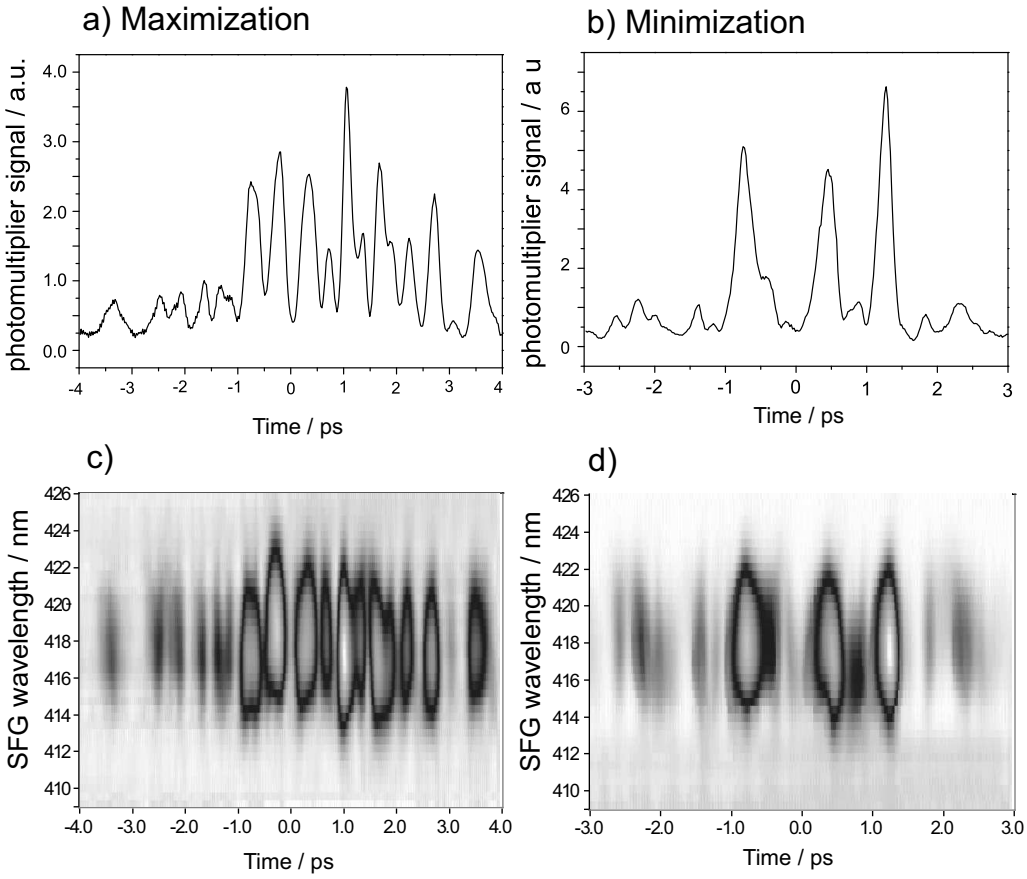

Figure 9.13: Cross-correlation and XFROG traces of the optimal pulses obtained for maximization and minimization of the ratio $\Re$ by employing phase-only modulation. Both cross-correlation traces for maximization (a) and minimization (b) exhibit a complex series of pronounced intensity maxima spread over ~ 5 ps and ~ 2.5 ps, respectively. The XFROG traces show the spectral and temporal intensity distribution for maximization (b) and minimization (d) as well. The laser wavelength was centered around 833 nm.

the optimal pulse for ratio minimization (Figure 9.12c).

The slightly higher factor obtained for phase-only modulation experiments demonstrates that the phase has not a high effect, but it is interesting that there is an effect! The phase can contribute to the optimized process by creating appropriate frequencies at the right times. A deeper insight in the mechanism can be achieved by amplitude-only modulation (see section 9.5.3).

In a phase-only optimization experiment, the transmission pattern of the modulator is not affected, i.e. the spectrum of the optimized pulse retains its

shape. The employed laser power of 330 mW remained constant as well.

Figure 9.13 displays the cross-correlation and XFROG traces obtained for maximization and minimization of the isotope ion ratio by phase-only modulation. Whereas the optimal pulses for maximization (Figure 9.13a and Figure 9.13c) show a series of intensity maxima (subpulses), the optimal pulse for minimization spread over 5 ps (Figure 9.13c and Figure 9.13d) reveals three pronounced subpulses. The measured XFROGs are difficult to interpret, but general information can be extracted. The subpulses in both optimal pulses in Figure 9.13c and Figure 9.13d are frequently separated by a multiple of half-period of oscillation in the $A^1\Sigma_u^+$ potential which is $\frac{1}{2}T_{osc} = 250$ fs. This can be explained, like in the previous section, by a stepwise excitation: the dimers are excited at the inner turning point of the $A^1\Sigma_u^+$ state. After a half oscillation period (250 fs), another excitation step follows at the outer turning point. This is achieved by temporal modulation, whereby the transmission remains constant.

From the phase-only optimization of the isotope ratio, the contribution of the phase to the selective ionization process is observed. The factor is comparably low with respect to the combined phase and amplitude experiments (section 9.5.1), but an optimization factor between ratio maximization and minimization is evident. The reason is currently not clear, but interference effects between propagating wave packets on the electronic excited states could be responsible. Thus it is expected that the amplitude modulation plays a major role for the high isotope selection.

9.5.3 Amplitude Modulation at 833 nm

This section focuses on the isotope selective ionization of the potassium dimers $^{39,39}K_2$ and $^{39,41}K_2$ by optimal control where only the amplitude of the input laser field is optimized by the feedback loop. By performing amplitude-only optimization, no temporal evolution of wave packets in the excited states occurs. This allows the exclusive observation of the particular transitions to the involved electronic excited states within the frequency pattern. The optimized pathway is expected to be different than in the phase-only experiments (or in the combined phase and amplitude modulation). The goal of the experiment is to find out if the amplitude modulation is most decisive in the isotope ratio control experiments performed in section 9.5.1.

Figure 9.14 shows the progression of the ion signal ratio $\Re$ during maximization (Figure 9.14a) and minimization (Figure 9.14b) of the isotope ratio as a function of the iteration number.

For maximization, the isotope ratio increased to $\Re_{max} = 37$, whereby an optimization factor of $\Re_{max}/\Re_n = 5.4$ is achieved. For minimization mea-

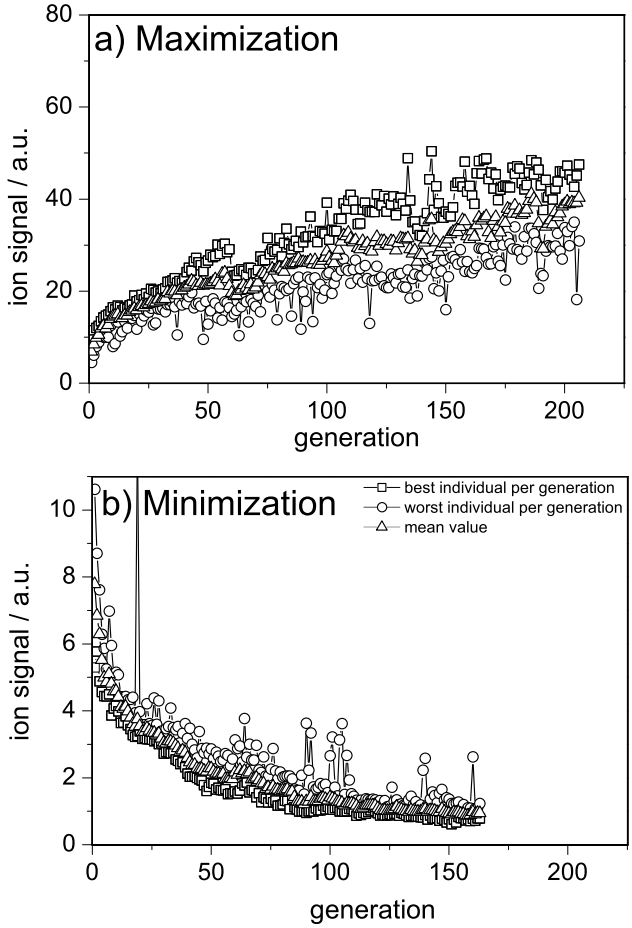

Figure 9.14: Evolution of the ion signal ratio $\Re$ =I($^{39,39}K_2$)/I($^{39,41}K_2$) during amplitude only optimization. (a) Evolution during ratio maximization, whereby a ratio $\Re_{max} = 37$ was achieved. (b) Evolution during ratio minimization, whereby the ratio is reversed to $\Re_{min} = 0.9$. The isotope ratio $\Re$ is modified by a total factor of $\Re_{max}/\Re_{min}$= 41 (see also the mass spectra in Figure 9.15). The squares represent the evolution of the best individual within a generation, the circles the evolution of the worst individual and the triangles their mean value.

surements, the isotope ratio was reversed to $\Re_{min} = 0.9$, leading to an optimization factor of $\Re_{min}/\Re_n = 0.13$. The total variation of the isotope ratio between maximization and minimization amounts $\Re_{max}/\Re_{min} = 41$. Thus the amplitude modulation plays an essential part in the selective isotope ionization.

By multiplying the optimization factors obtained for total variation of $\Re$ for phase and for amplitude separately one obtains $2.5 \times 41 = 102.5$ which

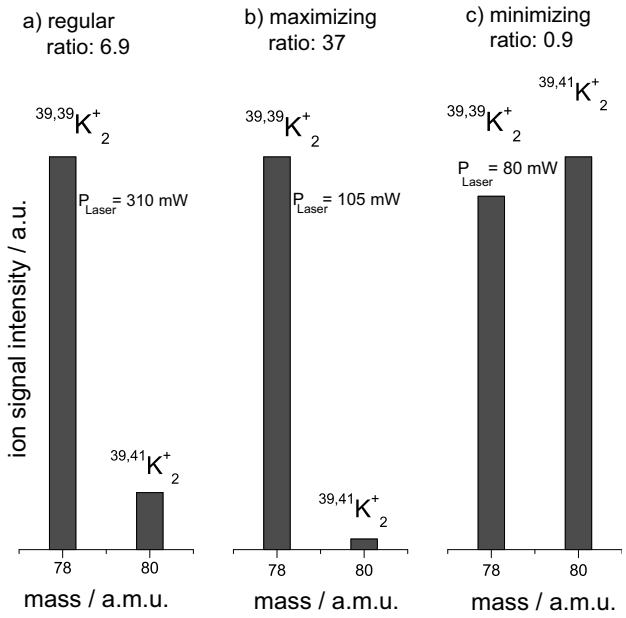

Figure 9.15: Mass spectra recorded by multi-photon ionization for the amplitude-only optimization. (a) Mass spectrum measured with a short pulse before the optimization experiment. (b) Mass spectrum recorded with the optimal pulse obtained for maximization. (c) Mass spectrum taken with the optimal pulse for minimization. The average laser power before the experiment (a), after ratio maximization (b) and ratio minimization (c) is given as well.

is smaller than the total variation factor observed in combined phase and amplitude modulation of 141. Thus the combined effect is more pronounced than pure phase and pure amplitude modulation.

The mass spectra are recorded with a single non-optimized pulse (Figure 9.15a), with the optimal pulse for maximization (Figure 9.15b) and minimization (Figure 9.15c), respectively. As expected the laser power decreases considerably due to the strong amplitude modulation. The average laser power before the optimization is 310 mW. After maximizing the isotope ion ratio the power decreases to 105 mW, whereas for minimization the laser power is reduced to 80 mW.

The spectra of the optimal pulses obtained for both maximization and minimization are displayed in Figure 9.16. As expected, both spectra reveal dominant peaks of different intensities. The intensity goes almost to zero between the peaks. For maximization (Figure 9.16a) the spectrum of the optimal pulse shows distinct peaks, which can be associated with transitions between the vibrational levels of the electronic ground state $X^1\Sigma_g^+$ and the

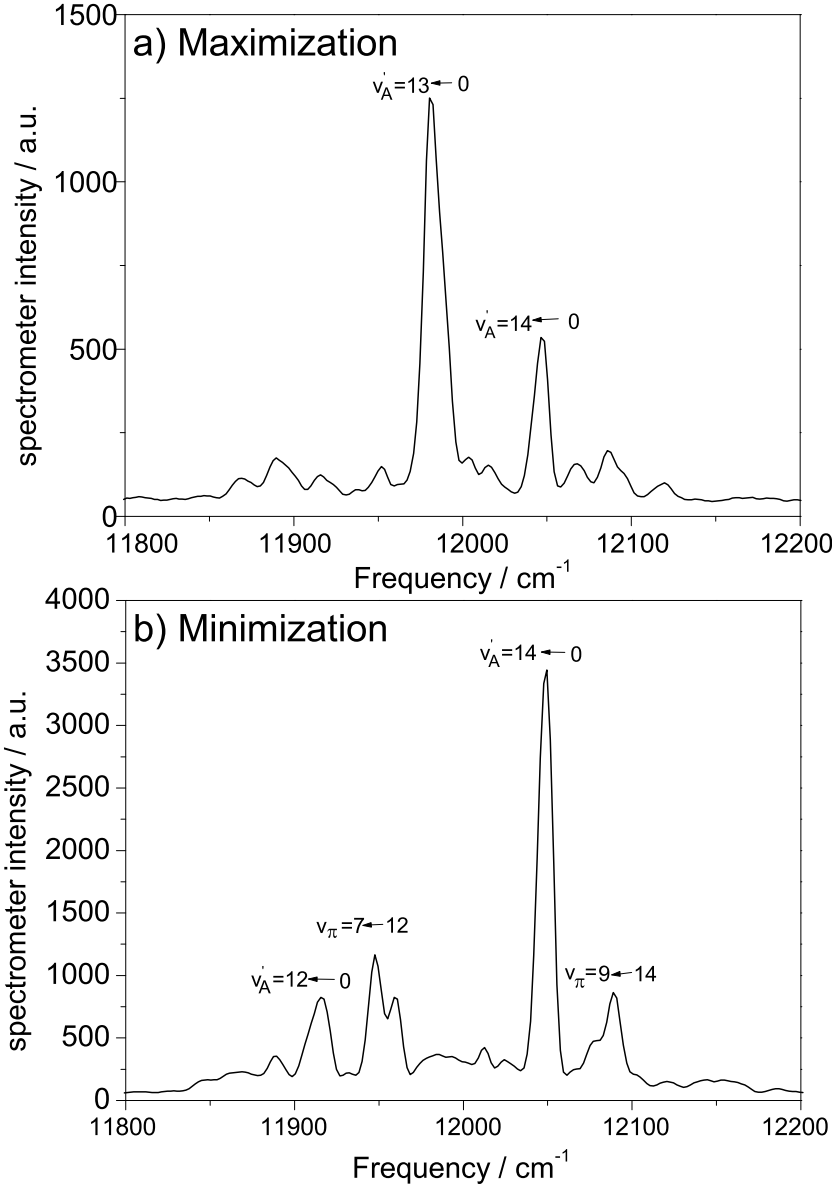

Figure 9.16: Spectra of the optimal pulses obtained for maximization (a) and minimization (b) of the ratio $\Re$ by employing a single-pulse amplitude-only modulation. The pronounced structures in the spectra can be assigned to transitions between different vibrational levels on the involved electronic excited states $X^1\Sigma_g^+$, $A^1\Sigma_u^+$, and $2^1\Pi_g$ of the $^{39,39}K_2$ isotope (a) and of the $^{39,41}K_2$ isotope (b). The central wavelength is 833 nm. The transmission pixel pattern of the modulator coincides with the sharp peaks in both spectra, respectively.

	Frequency / cm^{-1}			
Transition	**Maximization**	Theory	**Minimization**	Theory
$v_A^{'} = 12 \leftarrow 0$	—	—	11915	11909
$v_A^{'} = 13 \leftarrow 0$	11982	11986	—	—
$v_A^{'} = 14 \leftarrow 0$	12048	12051	12047	12039
$v_\pi^{'} = 9 \leftarrow 14$	—	—	12091	12097
$v_\pi^{'} = 7 \leftarrow 12$	—	—	11948	11948

Table 9.3: The identified frequencies observed in the optimal pulse spectra in Figure 9.16 for ion ratio optimization of the two K_2 isotopes for both maximization and minimization by amplitude-only modulation. The frequencies correspond to transitions between the indicated vibrational levels of the $X^1\Sigma_g^+$, $A^1\Sigma_u^+$, and $2^1\Pi_g$ electronic excites states. The theoretical values are taken from Ref. [81]

$A^1\Sigma_u^+$ excited state. The transitions involved are $v'_A = 13, 14 \leftarrow 0$. The transition $v'_A = 12 \leftarrow 0$ is completely missing.

In the case of minimization (Figure 9.16b) sharp peaks are also observed. The most intensive peaks are associated with transitions between the same ground state $X^1\Sigma_g^+$ and excited state $A^1\Sigma_u^+$. The transitions between these two states take place between the $v'_A = 12, 14 \leftarrow 0$ vibrational levels. One immediately notices that the peak assigned to $v'_A = 13 \leftarrow 0$ is missing in the spectrum for minimization. The presence of the sharp peaks at different frequencies in the optimal pulse spectra for ratio maximization and minimization accounts for the high isotope selection in which the evolutionary algorithm chooses the optimal vibrational levels of different electronic states in order to optically separate the two potassium dimer isotopes. Some of the peaks can be associated with transitions to vibrational levels of the $2^1\Pi_g$ excited state. These vibrational levels are estimated by calculating the time-independent Schrödinger equation numerically (see Ref. [80]). The estimated transitions are between the following vibrational levels of the $A^1\Sigma_u^+$ state and $2^1\Pi_g$ state: $v_\pi = 9 \leftarrow 14$ and $v_\pi = 7 \leftarrow 12$. The peak observed at 11959 cm^{-1} in Figure 9.16b remains currently unassigned.

The frequencies resolved from the spectra in Figure 9.16 are summarized in Table 9.3.

The cross-correlations and the XFROG traces of the optimal pulses for both maximization and minimization, respectively, are shown in Figure 9.17. The cross-correlation measurements recorded after maximization (Figure 9.17a) and minimization (Figure 9.17b) do not consist of a series of subpulses, but a single, short pulse. This is because the phase-locking of

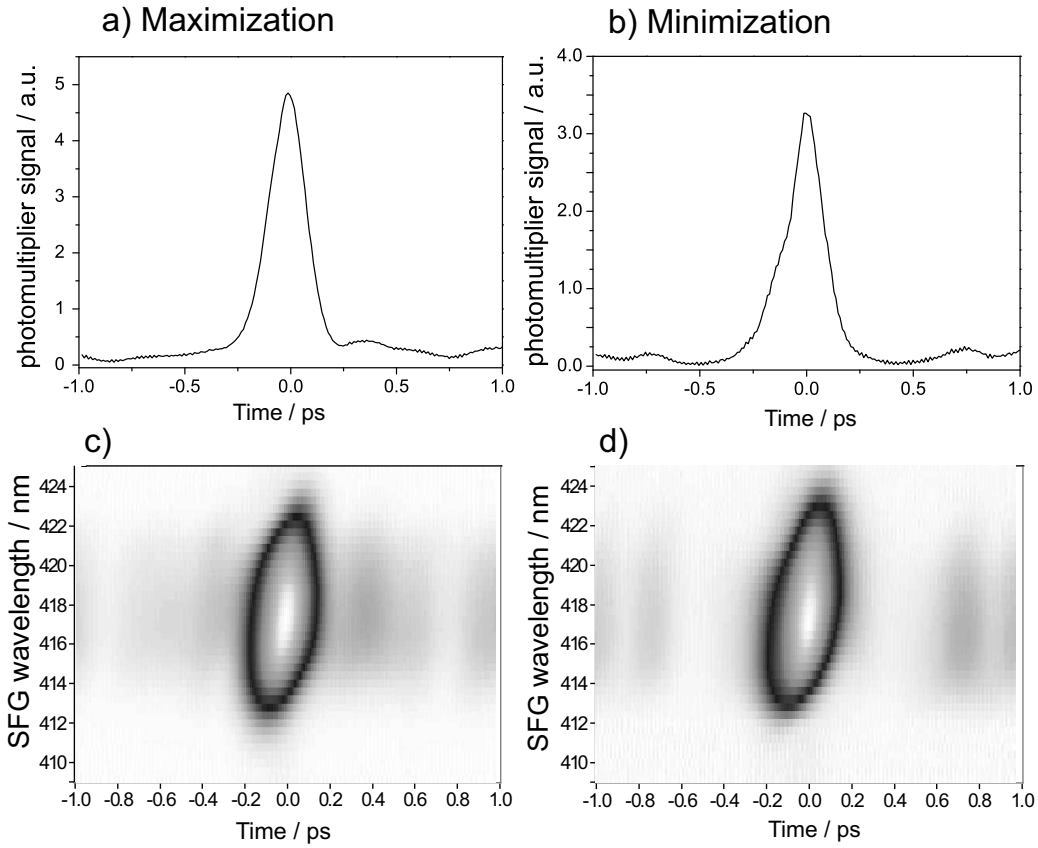

Figure 9.17: Cross-correlation and XFROG traces of the optimal pulses obtained for maximization and minimization of the ratio $\Re$ by employing single-pulse amplitude modulation. Both cross-correlation traces for maximization (a) and minimization (b) exhibit a single almost unshaped pulse. The XFROG traces for maximization (c) and minimization (d) reveal a short pulse, which is comparable to the input pulse in the shaping apparatus. The laser wavelength was centered around 833 nm.

the frequency components leads to their temporal superposition which is mirrored in the short pulse observed in the XFROG traces shown in Figure 9.17c and Figure 9.17d, respectively. The time duration[3] of the optimal pulse for maximization is $\Delta t_{max} = 200$ fs, whereas for minimization the pulse has $\Delta t_{max} = 220$ fs time bandwidth. This is comparable to the input laser pulse which has a temporal bandwidth of $\Delta t_{short} = 220$ fs.

[3]The bandwidth is measured at FWHM assuming the pulses have a Gaussian shape.

	Modulation		
Experiment/Factor	**Phase and Amplitude**	**Phase**	**Amplitude**
Maximization $\Re_{max}$	72	11	37
Minimization $\Re_{min}$	0.51	4.3	0.9
Total variation $\Re_{max}/\Re_{min}$	141	2.5	41

Table 9.4: The optimization factors obtained after different laser pulse modulation experiments. $\Re_{max}$ is the ion ratio after maximization, $\Re_{min}$ the ion ratio after minimization between the two potassium dimer isotopes $^{39,39}K_2$ and $^{39,41}K_2$, respectively. The regular ratio under the experimental conditions in the molecular beam is $\Re_n = 6.9$.

9.5.4 Discussion

The optimization factors obtained for the isotope selective ionization performed at 833 nm are summarized in Table 9.4. In the following section a the results obtained for phase-only and for amplitude-only modulation are compared to the combined phase and amplitude modulation experiments.

Amplitude-only vs. Combined Phase and Amplitude

In the amplitude-only modulation the temporal evolution of the wave packet is obstructed and can be considered as a restricted optimization. Due the short interaction time the wave packet can not propagate far in the $A^1\Sigma_u^+$ excited state. Thus the transition between the $A^1\Sigma_u^+$ and $2^1\Pi_g$ states occurs close to the inner turning point of the $2^1\Pi_g$ potential, as depicted in Figure 9.18. In order to resonantly reach the $2^1\Pi_g$ excited state within the ionization step from the $A^1\Sigma_u^+$ state, the evolutionary algorithm should employ higher frequencies and renounce to the $v_A^{'} = 12 \leftarrow 0$ transition. This could explain the missing peak in Figure 9.16a. Since only the population in the $2^1\Pi_g$ excited state is relevant for the isotope selectivity, it is expected that the efficiency of the method is reduced.

The peaks which are associated with intermediate transitions between the $2^1\Pi_g \leftarrow A^1\Sigma_u^+$ excited states are not predominant or even missing from the spectra obtained for the pure amplitude experiment. This can be understood by the fact that in the isotope selection process, the second excitation step plays a minor role than in the combined phase and amplitude case.

In the phase and amplitude experiments, the temporal separation between several neighboring subpulses amounts ~ 250 fs, which represents half of the oscillation period of the wave packet on the $A^1\Sigma_u^+$ excited state. Apparently, a consecutive excitation at the inner turning point of the $A^1\Sigma_u^+$ potential

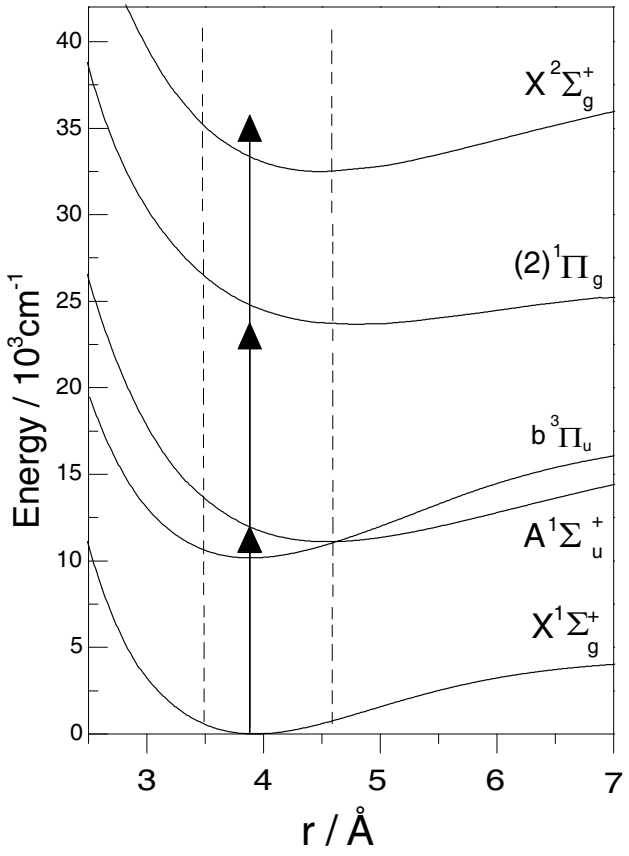

Figure 9.18: The optimized ionization path for in the pure amplitude optimization experiments of the $^{39,39}K_2/^{39,41}K_2$ ionization ratio. The time evolution of the wave packet on the electronic excited states is strongly hindered. The feedback-loop needs to select higher frequencies for a successful transition between the vibrational levels of the $A^1\Sigma_u^+$ and $2^1\Pi_g$ states (the second excitation step).

takes place followed by a second excitation from the outer turning point (after 250 fs) of the $A^1\Sigma_u^+$ state (see Figure 9.19). The time separation existing between the two excitation steps in phase and amplitude optimizations permits temporal modulation of the spectral components. Thus the frequencies responsible for the first excitation step are decreased when the subpulse for the second excitation arrives. On the other hand, the spectral components responsible for the second excitation are increased when the subpulse which performs the first excitation step is less intense. The alternation between frequency components for the first excitation and subpulses for the second excitation is responsible for the high isotope selectivity, compared to the

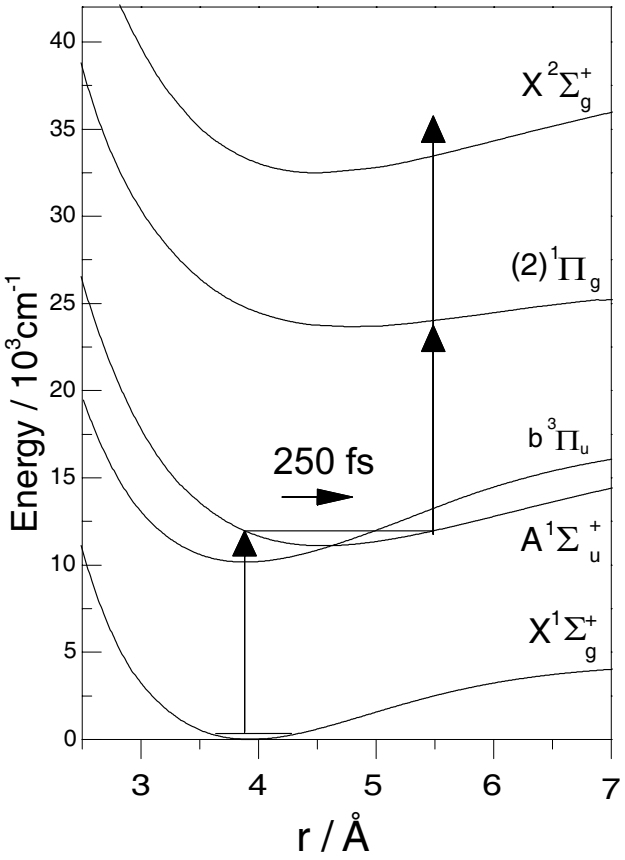

Figure 9.19: The optimized ionization path in the phase-only and combined phase and amplitude optimization experiments of the $^{39,39}K_2/^{39,41}K_2$ ionization ratio. The population is transferred from the ground state to the $A^1\Sigma_u^+$ excited state. After a time delay of $\frac{1}{2}T_{osc} = 250$ fs a transfer of population from the $A^1\Sigma_u^+$ state to the ionic state via the $2^1\Pi_g$ state takes place.

amplitude-only optimizations. This demonstrates the efficiency of combined phase and amplitude modulation, in particular the effect of temporal pulse modulation.

Phase-only vs. Combined Phase and Amplitude

The variation between maximization and minimization factors obtained for phase-only modulation is $\Re_{max}/\Re_{min} = 2.5$ (section 9.5.2). Compared to the total factor for combined phase and amplitude at 833 nm ($\Re_{max}/\Re_{min} = 141$), it shows that the phase-only optimization is less efficient in the isotope selection process. Although no frequency modulation occurs, the pure phase

modulation provides higher variation factor than in pump–probe measurements and the two-pulse optimization. (Here, the isotope ratio was changed by a factor of 1.6 and 1.9, respectively.)

The optimal pulses reveal in both maximization and minimization cases a series of subpulses separated often by a multiple of 250 fs, which represents $n \cdot \frac{1}{2}T_{osc}$ of the $A^1\Sigma_u^+$ state. The subpulses separated by 250 fs, 500 fs, 750 fs may lead to constructive and destructive interferences of the propagating wave packets [167] during the ionization process. These interferences are isotope dependent and could contribute to the isotope selective ionization efficiency. For example, if a subpulse in the optimal pulse form is generated over more than an oscillation period, the wave packet can return to its excitation position, where the laser pulse is still present. Depending on the phase difference between individual intensity maxima, destructive interferences for one isotope and constructive interferences for the other one or vice versa could occur. This may take place either on the $A^1\Sigma_u^+$ excited state, but also on the $2^1\Pi_g$ state, which is resonant to the employed laser frequency on the involved ionization pathway.

By comparing the cross-correlation traces for phase-only (Figure 9.13) and phase and amplitude experiments (Figure 9.10) one can notice similarities in the pulse forms. This gives hints about an alike temporal evolution of the wave packet on the potentials of the corresponding electronic excited states.

Finally, a short remark: the isotope separation method developed during this work does effectively minimize or maximize the isotope ion ratio, but does not increase the total number of ions corresponding to a particular species. Due to the strong amplitude modulation, as seen in the recorded spectra, the total number of ions produced by the optimal pulse decreases in comparison with the ions produced by an short pulse. Only the isotope ratio is considerably altered.

9.5.5 Phase and Amplitude Modulation at 820 nm

The experiments on isotope selective ionization of potassium dimers by means of shaped femtosecond laser pulses is continued at lower wavelengths.

The goal of the experiment is to investigate if the series of transitions between different vibrational levels in the $A^1\Sigma_u^+$ state are present at other excitation wavelengths. By changing the laser wavelength, the optical excitation will take place on higher vibrational levels than the ones observed at 833 nm.

This section describes the experiments performed at 820 nm central wavelength, whereby both the phase and the amplitude of the laser field are modulated by passing through the liquid crystal mask.

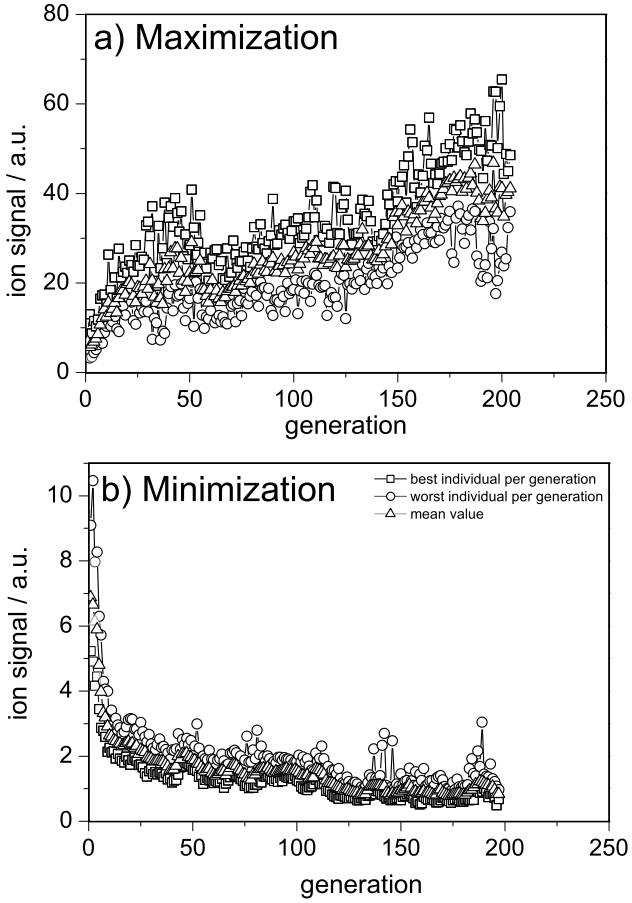

Figure 9.20: Progression of the ion signal ratio $\Re$ =I($^{39,39}K_2$)/I($^{39,41}K_2$) during single pulse optimization centered at 820 nm. (a) Progression during ratio maximization, whereby a ratio $\Re_{max} = 40$ was achieved. (b) Progression during ratio minimization, whereby the ratio is $\Re_{min} = 0.82$. The isotope ratio $\Re$ is modified by a total factor of $\Re_{max}/\Re_{min}$= 49. The squares represent the evolution of the best individual within a generation, the circles the evolution of the worst individual and the triangles their mean value. Hereby both phase and amplitude of the input light field are optimized.

The evolution of the ion signal ratio is shown in Figure 9.20 for both maximization and minimization of the ion ratio $\Re$ =I($^{39,39}K_2^+$)/I($^{39,41}K_2^+$). After the optimization algorithm reaches convergence, the ion ratio changes to $\Re_{max} = 40$ for maximization and to $\Re_{min} = 0.82$ for minimization, respectively. Also in this experiment for minimization, the ratio of the two isotopes is reversed. During the maximization experiment, the fluctuations in the molecular beam were ± 3–4 %. They may be the cause of the lower

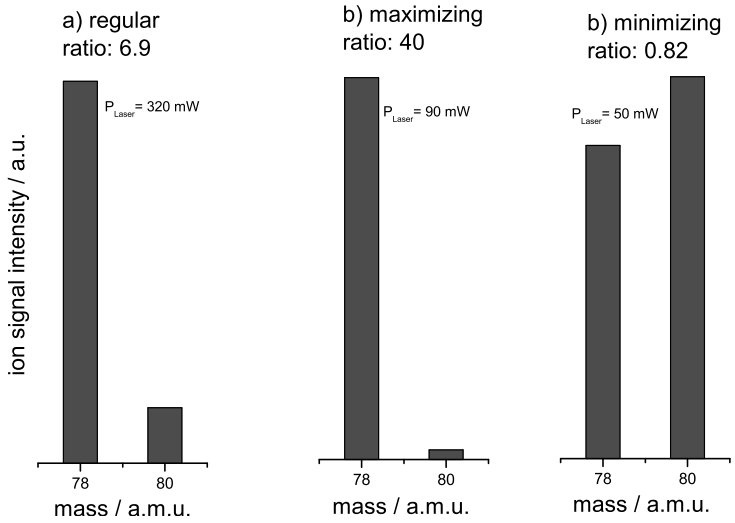

Figure 9.21: Mass spectra recorded with a short pulse before the isotope ion ratio optimization (a), with the optimal pulse obtained for ratio maximization (b) and with the optimal pulse for minimization (c) at a central wavelength of 820 nm. Hereby both the phase and amplitude of the laser pulse are modulated. The average laser power before the experiment (a), after ratio maximization (b) and ratio minimization (c) is given as well.

ion signal ratio produced by the best individual compared to the previous generation. This induces a decrease of the ion signal ratio in the evolution of the best individual, if additionally all other individuals generate less ion yield of both isotopes than the previous best one. Therefore the negative variations in the curves presented in Figure 9.20a can be explained.

Figure 9.21 shows the mass spectra recorded before the optimization experiment and after the ratio maximization and minimization, respectively. The average laser power before the optimization is 320 mW. After the maximization experiment only 90 mW exits the pulse shaping apparatus, whereas after minimization the average laser power is reduced to only 50 mW.

In order to understand the optimized process, optimal pulse spectra are recorded and displayed in Figure 9.22.

Similar to the previous optimal pulse spectra, they reveal distinct peaks with strong attenuation in between (in some cases almost down to zero). Apparently at 820 nm the isotope selective ionization takes place because of different transitions between vibrational levels of the electronic states $A^1\Sigma_u^+ \leftarrow X^1\Sigma_g^+$ and $2^1\Pi_g \leftarrow A^1\Sigma_u^+$ states. The transitions take place on levels with higher vibrational quantum numbers, as expected from the laser tuning to a higher central frequency. Some of the peaks can be associ-

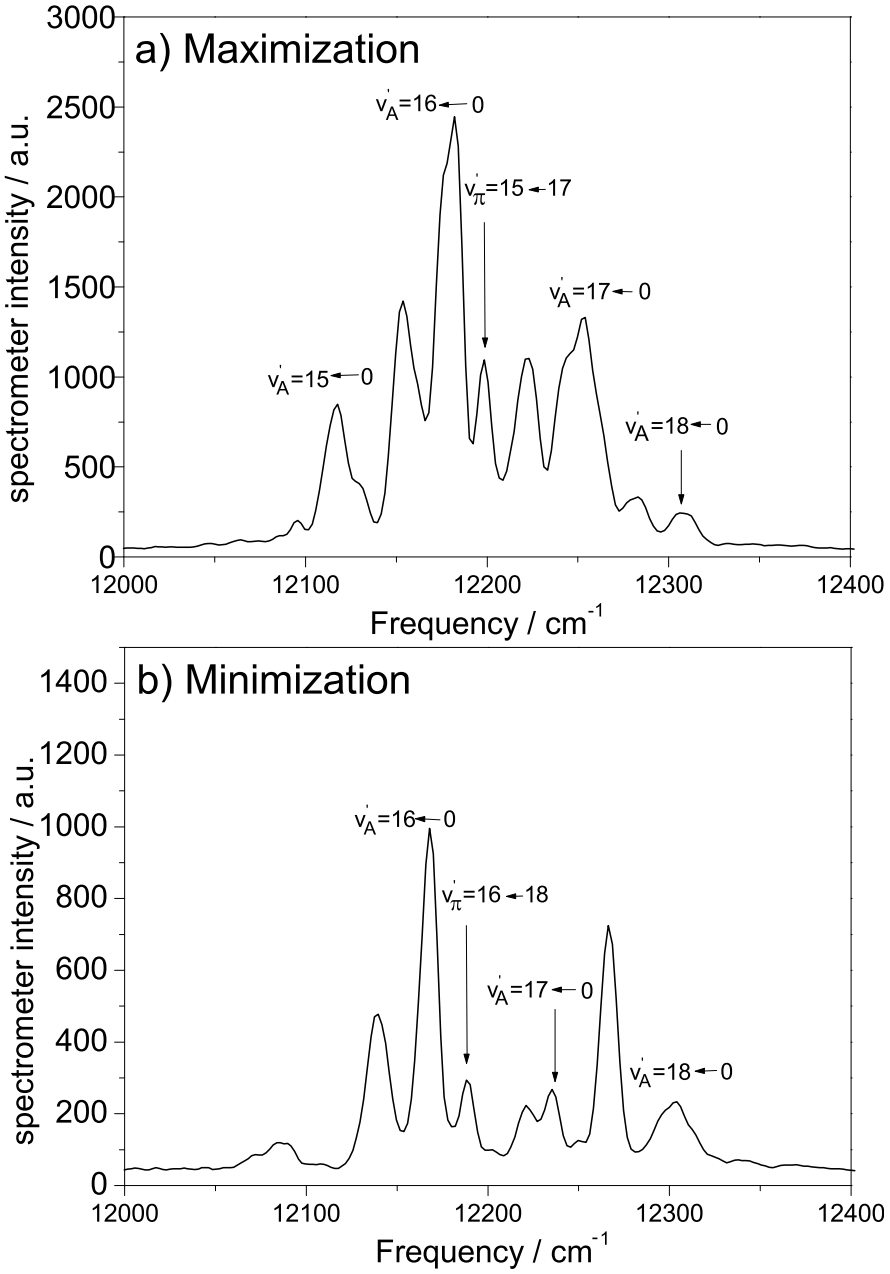

Figure 9.22: Optimal pulse spectra obtained for maximization (a) and minimization (b) of the ratio $\Re$ by employing phase and amplitude modulation at 820 nm. The distinct peaks in the spectra can be assigned to transitions between different vibrational levels of the electronic states $X^1\Sigma_g^+$, $A^1\Sigma_u^+$, and $2^1\Pi_g$ of the $^{39,39}K_2$ isotope (a) and of the $^{39,41}K_2$ isotope (b). The transmission pixel pattern of the modulator corresponds to the peaks observed in the optimal pulse spectra.

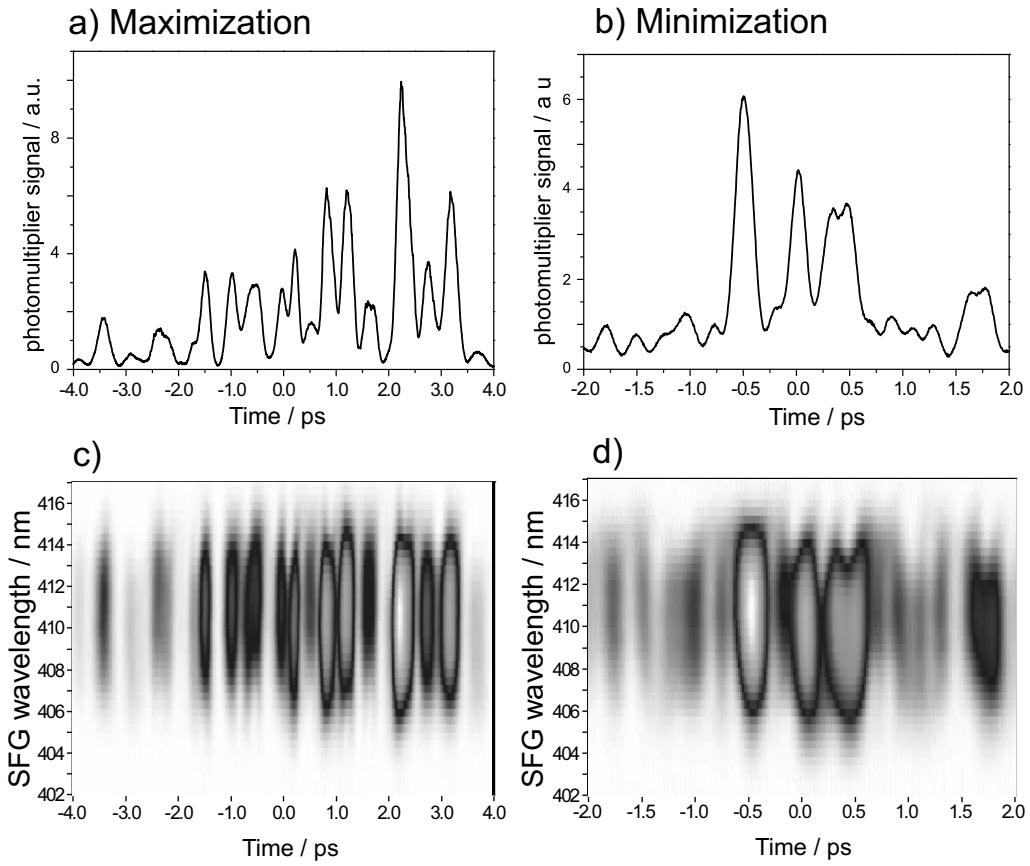

Figure 9.23: Cross-correlation and XFROG traces of the optimal pulses obtained for maximization and minimization of the ratio $\Re$ by employing the single-pulse optimization scheme. Both cross-correlation traces for maximization (a) and minimization (b) exhibit a complex series of pronounced intensity maxima spread over ~ 8 ps and ~ 4 ps, respectively. The spectral and temporal resolved cross-correlation traces (XFROG) for maximization (c) and minimization (d) are shown as well. The laser wavelength is centered around 820 nm.

ated with transitions from the ground electronic state to the $A^1\Sigma_u^+$ excited state: $v_A^{'} = 15, 16, 17, 18 \leftarrow 0$ for maximization (Figure 9.22a) and $v_A^{'} = 16, 17, 18 \leftarrow 0$ for minimization (Figure 9.22b), respectively. Transitions between particular vibrational levels of the $A^1\Sigma_u^+$ and $2^1\Pi_g$ states are observed in the optimal pulse spectra as well: $v_\pi^{'} = 15 \leftarrow 17$ for maximization (Figure 9.22a) and $v_\pi^{'} = 16 \leftarrow 18$ for minimization (Figure 9.22b).

The resolved frequencies from the spectra in Figure 9.22 corresponding to particular vibrational levels between the involved electronic states are

	Frequency / cm^{-1}			
Transition	**Maximization**	Theory	**Minimization**	Theory
$v_A' = 15 \leftarrow 0$	12116	12117	—	—
$v_A' = 16 \leftarrow 0$	12182	12182	12167	12168
$v_A' = 17 \leftarrow 0$	12251	12248	12235	12233
$v_A' = 18 \leftarrow 0$	12309	12312	12300	12297
$v_\pi' = 15 \leftarrow 17$	12199	12204	—	—
$v_\pi' = 16 \leftarrow 18$	—	—	12189	12194

Table 9.5: The identified frequencies observed in the optimal pulse spectra in Figure 9.22 for ion ratio optimization of the two K_2 isotopes for both maximization and minimization by phase and amplitude modulation at 820 nm. The frequencies correspond to transitions between the indicated vibrational levels of the $X^1\Sigma_g^+$, $A^1\Sigma_u^+$, and $2^1\Pi_g$ electronic states. The theoretical values are taken based on the calculations in Ref. [81].

summarized in Table 9.5. For minimization the levels are shifted on average by 14 cm^{-1} [81, 166].

Cross-correlations and the XFROG traces of the optimal pulses for both maximization and minimization, respectively, are recorded and shown in Figure 9.23. The cross-correlation measurements recorded after maximization (Figure 9.17a) reveal a series of intensity maxima whereas for minimization (Figure 9.17b) only three dominant peaks are observed. No accurate explanation of the temporal pulse shapes and of the XFROG traces can be given, but general remarks can be made. As observed in previous experiments, the subpulses are often separated by $n \cdot \frac{1}{2}T_{osc}^{K_2}$ (a multiple of half of oscillation period) of the $A^1\Sigma_u^+$ excited state[4]. This can be explained similar to the previous experiments at 833 nm by a stepwise excitation process: excitation at the inner turning point of the $A^1\Sigma_u^+$ state, followed after 250 fs by an excitation at the outer turning point. This statement is supported by the known fact that at the outer turning point the Franck-Condon window is favorable for a resonant transition to the $2^1\Pi_g$ state (see Figure 9.1 and Refs. [53, 80]) on the ionization path.

[4]The excitation wavelength is changed to 820 nm with respect to 833 nm used in previous measurements; thus higher vibrational levels in the $A^1\Sigma_u^+$ excited state are reached. Since no pump–probe measurements were done at this wavelength, the vibrational period of the wave packet on the $A^1\Sigma_u^+$ excited state of the potassium dimers is estimated to be $T_{osc} \approx 500$ fs.

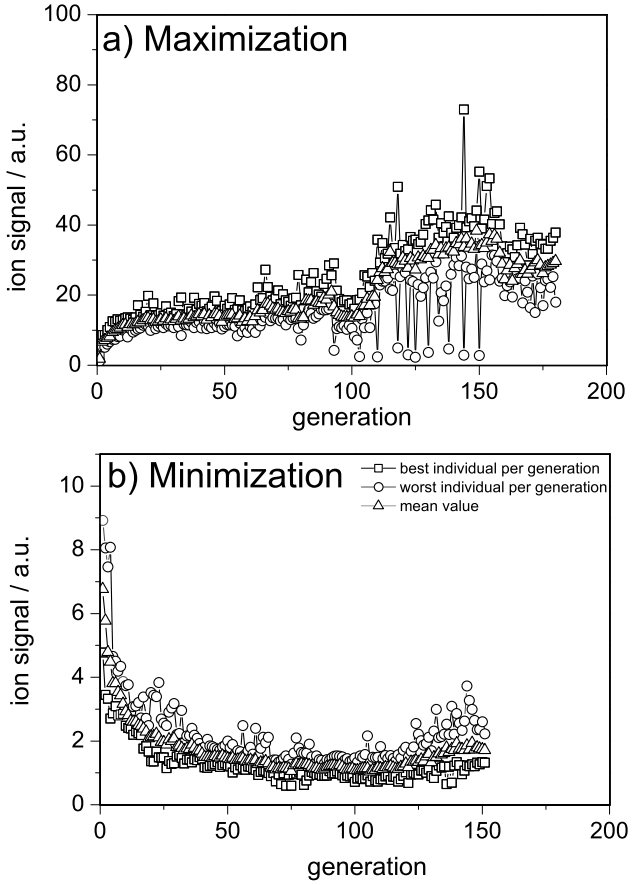

Figure 9.24: Progression of the ion signal ratio $\Re = I(^{39,39}K_2)/I(^{39,41}K_2)$ during single pulse optimization centered at 810 nm. (a) Progression during ratio maximization, whereby a ratio $\Re_{max} = 24.8$ was achieved. (b) Progression during ratio minimization, whereby the ratio is $\Re_{min} = 1.8$. The isotope ratio $\Re$ is modified by a total factor of $\Re_{max}/\Re_{min} = 13.8$. The squares represent the evolution of the best individual within a generation, the circles the evolution of the worst individual and the triangles their mean value. Hereby both phase and amplitude of the input light field are optimized.

9.5.6 Phase and Amplitude Modulation at 810 nm

The experiment described in this section was performed at 810 nm laser central wavelength. The measurements are investigating whether the method of isotope ratio control is valid at even lower excitation wavelengths, which are relatively far from the previously used 833 nm. Hereby even higher vibrational levels in the $A^1\Sigma_u^+$ potential are expected to be populated. The goal is to learn about the optimized process from the acquired optimal pulse shapes.

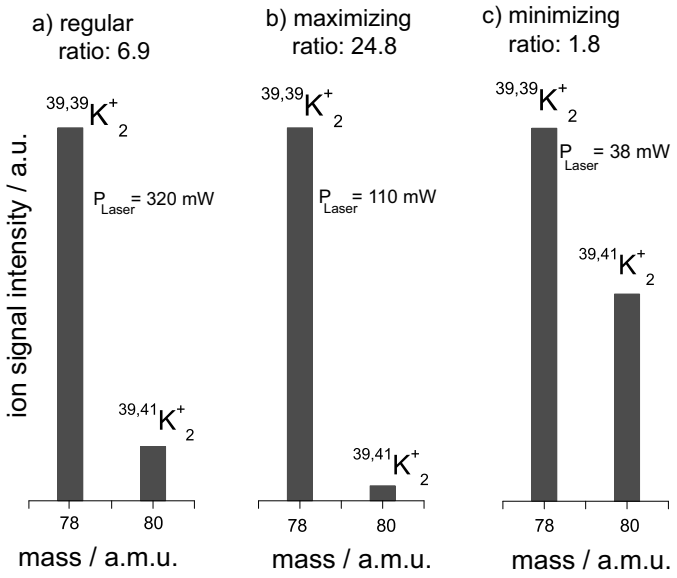

Figure 9.25: Mass spectra of the molecular beam containing only potassium dimers recorded by laser multi-photon ionization before optimization (a), after the ion ratio maximization (b) and after isotope ion ratio minimization (c). Hereby both phase and modulation of the laser pulse were modulated. The average laser power before the experiment (a), after ratio maximization (b) and ratio minimization (c) is given as well. The wavelength is centered at 810 nm

The curves in Figure 9.24 show the evolution of the ion signal ratio $\Re$ =I($^{39,39}K_2$)/I($^{39,41}K_2$) during the maximization and minimization of one potassium dimer isotope versus the other. Hereby the ratio $\Re$ served as feedback signal for the evolutionary algorithm, too. A progressive increase is observed for maximization (Figure 9.24a), whereby the ion signal ratio increase to $\Re_{max} = 24.8$ from the regular value of $\Re_n = 6.9$. Thereby an optimization factor of $\Re_{max}/\Re_n = 3.6$ is achieved. Although instabilities of about $\pm 7\%$ are present in the cluster beam, the algorithm is able to converge, even if during the optimization the best individual in one generation might produce a lower ion signal in the next generation. (Around the 90^{th} generation a decrease is observed. After the 110^{th} iteration the ion signal ratio returns the same value.) In the case of minimization, the ion signal ratio converged to the value $\Re_{min} = 1.8$. Thus the overall variation of the isotope ratio between maximization and minimization experiments is $\Re_{max}/\Re_{min} = 13.8$.

The mass spectra, displayed in Figure 9.25, confirm the obtained results for the optimization factors. The mass spectrum recorded with an short laser beam of average laser power of 320 mW is shown in Figure 9.25a. After

	Frequency / cm^{-1}			
Transition	**Maximization**	Theory	**Minimization**	Theory
$v_A^{'} = 18 \leftarrow 0$	12312	12312	12300	12297
$v_A^{'} = 19 \leftarrow 0$	12372	12373	12359	12357
$v_A^{'} = 20 \leftarrow 0$	12434	12437	12411	12420

Table 9.6: The identified frequencies observed in the optimal pulse spectra in Figure 9.26 for ion ratio optimization of the two K_2 isotopes for both maximization and minimization by phase and amplitude modulation at 810 nm. The frequencies correspond to transitions between the indicated vibrational levels of the $X^1\Sigma_g^+$ and $A^1\Sigma_u^+$ electronic states. The theoretical values are taken from [81, 166].

the isotope ratio maximization (Figure 9.25a) the laser power is reduced to 110 mW. The mass spectrum in Figure 9.25c is recorded with the optimal pulse obtained for minimizing the isotope ion ratio, whereby the laser power decreased to only 38 mW.

The spectra of the optimal pulses are shown in Figure 9.26 for both maximization and minimization cases. Only a few pronounced peaks can be distinguished.

The main peaks for maximization can be assigned to transitions between vibrational levels of the involved states in the ionization process: $X^1\Sigma_g^+$ and $A^1\Sigma_u^+$ electronic states. For the ratio maximization transitions $v_A^{'} = 18, 19 \leftarrow 0$ are the most important for the excitation process (Figure 9.26a). As expected the excitation occurs on higher vibrational levels of the $A^1\Sigma_u^+$ state.

The spectrum of the optimal pulse for minimization (Figure 9.26b) consists of mainly one distinct peak, corresponding to the $v_A^{'} = 19 \leftarrow 0$ transition between the $X^1\Sigma_g^+$ and $A^1\Sigma_u^+$ states. Transitions between $v_A^{'} = 18 \leftarrow 0$ and $v_A^{'} = 20 \leftarrow 0$ occur as well, but they are less intense. Several peaks of low intensity remain at this point unassigned.

The frequencies corresponding to the levels identified in the optimal pulse spectra are summarized in Table 9.6. The sharp peaks for minimization are located at different frequencies compared to the corresponding peaks observed for minimization. They are shifted on average by 16 cm^{-1}.

The cross-correlations of the optimal pulses for both maximization and minimization are measured together with the corresponding XFROG traces (see Figure 9.27). They reveal a series of subpulses spread over ~ 4 ps and ~ 5 ps, respectively (Figure 9.27a and Figure 9.27b). Most of the subpulses in the XFROG traces correspond to short pulses, but in few cases pulses

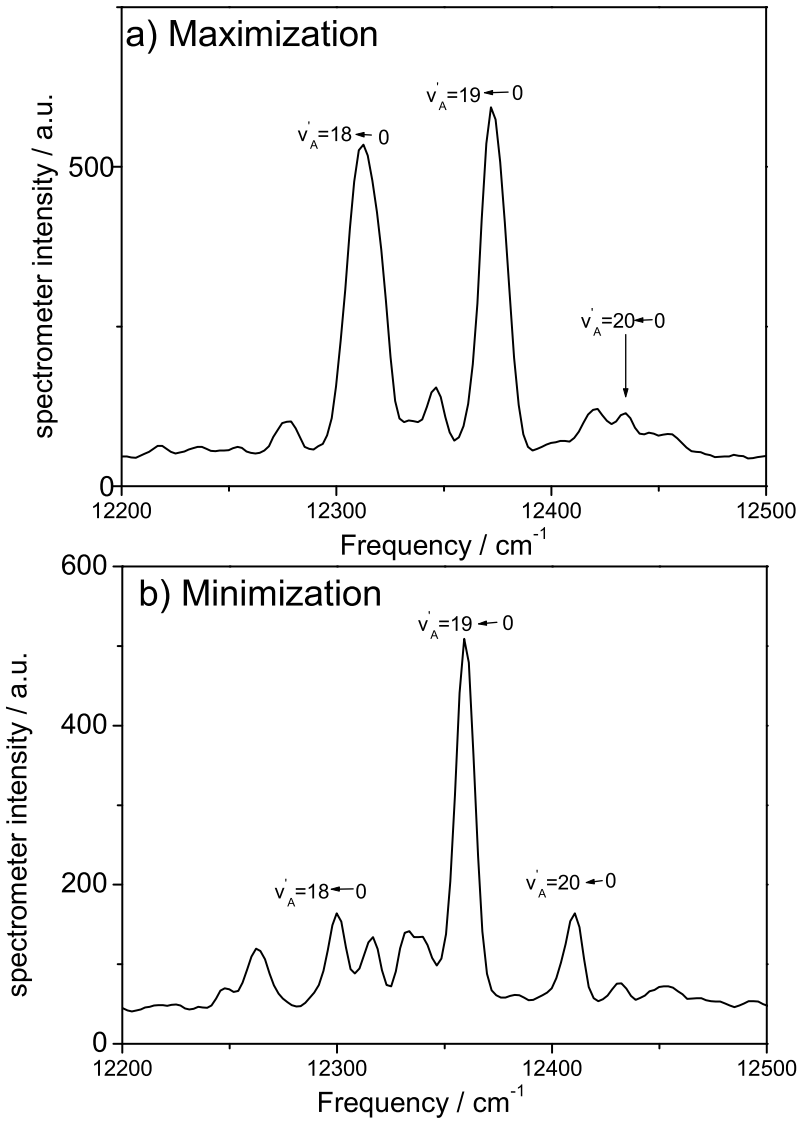

Figure 9.26: The spectra of the optimal pulse obtained for maximization (a) and minimization (b) of the isotope ion ratio $\Re$ by employing phase and amplitude modulation at 810 nm. The dominant peaks in the spectra can be assigned to transitions between different vibrational levels of the electronic states $X^1\Sigma_g^+$, $A^1\Sigma_u^+$ of the $^{39,39}K_2$ isotope (a) and of the $^{39,41}K_2$ isotope (b). The transmission pixel pattern on the modulator corresponds to the peaks in the optimal pulse spectra, respectively.

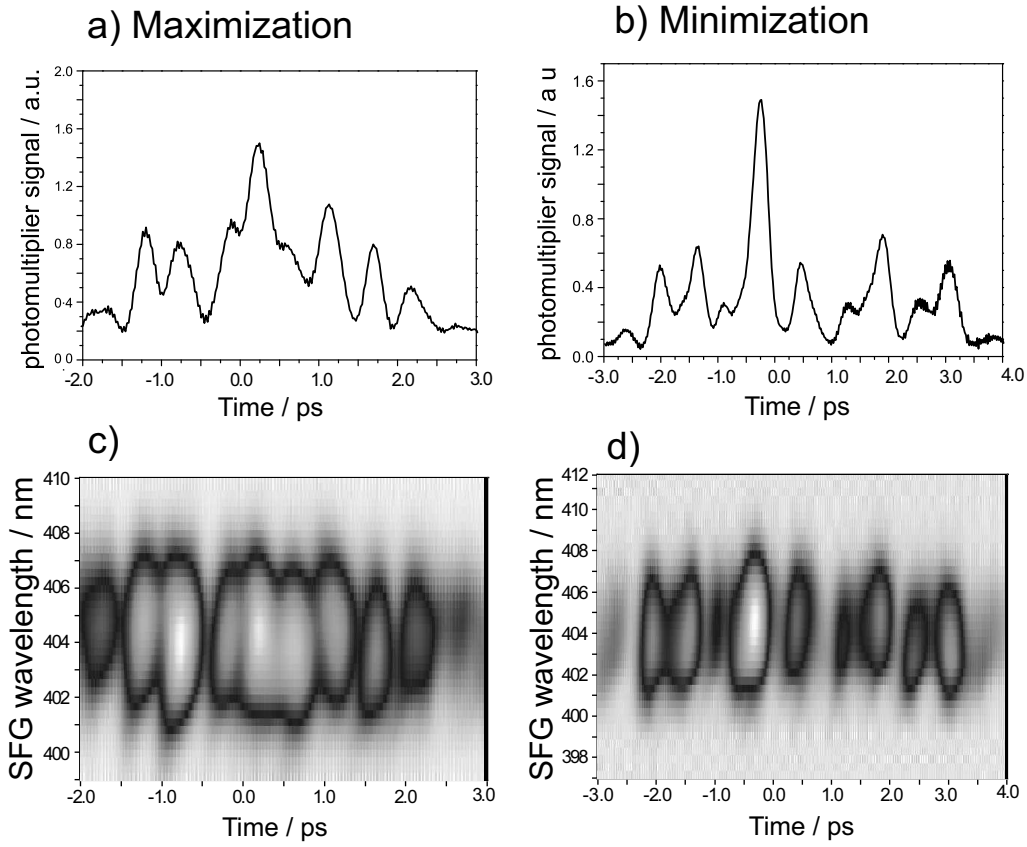

Figure 9.27: Cross-correlation and XFROG traces of the optimal pulses obtained for maximization and minimization of the ratio $\Re$ by employing the single-pulse optimization scheme. Both cross-correlation traces for maximization (a) and minimization (b) exhibit a complex series of pronounced intensity maxima spread over $\sim$ 4 ps and $\sim$ 5 ps, respectively. The spectral and temporal resolved cross-correlation traces (XFROG) for maximization (c) and minimization (d) are shown as well. The laser wavelength was centered around 810 nm.

containing small positive or negative chirps are present. It stands out again that in most of the subpulse separations there is a multiple of $\frac{1}{2}T_{osc}$ in the $A^1\Sigma_u^+$ state[5]. This can lead to a similar stepwise excitation process, as dis-

[5]Higher vibrational levels in the $A^1\Sigma_u^+$ excited state are reached due to the tuning of the excitation wavelength is to 810 nm (compared to the experiments performed at 833 nm). Since no pump–probe measurements were done at this wavelength, the vibrational period of the wave packet on the $A^1\Sigma_u^+$ excited state of the potassium dimers is estimated to be $T_{osc} \approx 500$ fs.

cussed in the previous sections. Thus an excitation at the inner turning point of the $A^1\Sigma_u^+$ potential can be followed by an excitation at the outer turning point. Subpulse distances of 500 fs are observed as well. This might be explained by the fact that after one oscillation period the algorithm waits one oscillation period in order to create another subpulse. This will enable an effective focussing of the wave packet from the inner turning point where the first excitation occurs to the outer turning point where the second excitation step takes place. The present interpretation is backed by the fact that the Franck-Condon window of ionization is most favorable at this nuclear distance, according to Figure 9.1 and Refs. [53, 80]. Furthermore, isotope-dependent constructive and destructive interferences between the generated wave packets [167] should not be neglected. They could increase the efficiency of the isotopic selection as well.

At this point it is not clear why the optimization factor at 810 nm is considerably lower than the optimization factor obtained at 833 nm. Since the isotope selectivity is expected to increase compared to the optimizations at 833 nm due to a larger isotope shift, the selectivity occurs mainly in the first excitation step, i.e. the transition $A^1\Sigma_u^+ \leftarrow X^1\Sigma_g^+$. The decrease of the optimization factor is more likely due to the second transition between the $A^1\Sigma_u^+$ and $2^1\Pi_g$ states.

9.6 Summary and Outlook

This chapter described a method which considerably alters the isotope ratio $\Re = I(^{39,39}K_2)/I(^{39,41}K_2)$ by employing evolution strategies in an optimization loop. The potassium dimer was chosen as a model system, but the method is expected to be feasible for other isotopic clusters or larger molecules as well. The results on NaK dimers ($^{23}Na^{39}K$ vs. $^{23}Na^{41}K$) demonstrated the potential of the applied method [163]. All the experimental parameters (the pixel resolution of the liquid crystal array(s), the laser bandwidth, the pulse duration) were set to fit the frequency resolution and required time evolution. The pulse peak intensity within the interaction region (less than 1 GW cm^{-2}) permits the optimization experiments to take place in the weak-field regime, which helps the interpretation of the acquired optimal pulses.

The method could be fast enough to avoid IVR opposite to the technique which uses wave packet recurrence phenomena. Hence information about the wave packet dynamics during IVR could be gained. Compared to the isotope separation method by cw lasers, the advantage of this method is assured by the broad laser bandwidth. This allows total isotope selection of the system where several vibrational levels are initially populated, versus single state se-

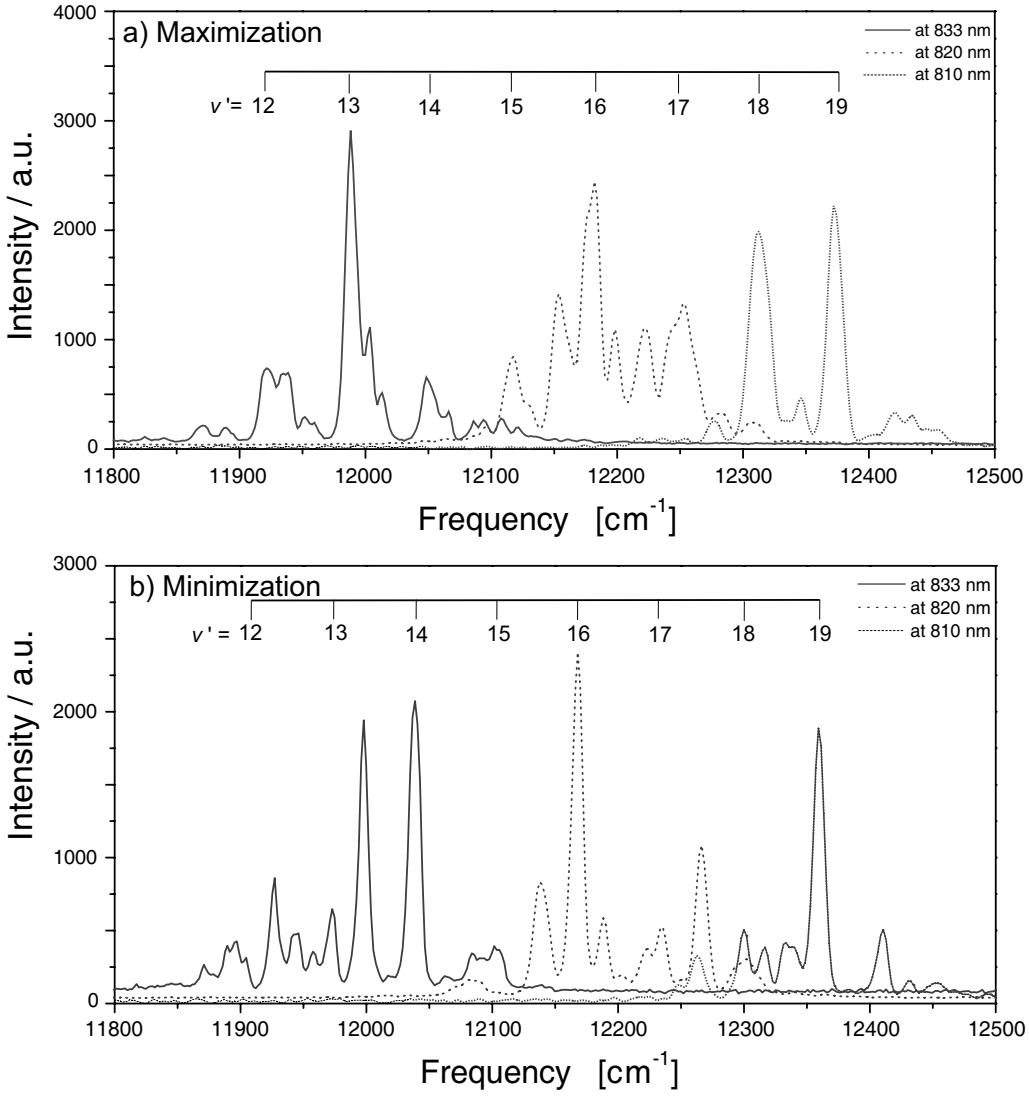

Figure 9.28: Optimal pulse spectra obtained for the maximization (a) and for minimization (b) of the isotope ratio $\Re = I(^{39,39}\mathrm{K}_2)/I(^{39,41}\mathrm{K}_2)$ at 833 nm, 820 nm and 810 nm. As highlighted, some of the sharp peaks can be associated with different transitions between the electronic ground state $\mathrm{X}^1\Sigma_g^+$ and the excited state $\mathrm{A}^1\Sigma_u^+$.

lection with cw lasers. Ionization of the investigated system is not necessary. Isotope specific excited states could be as well selectively populated, leading to a possibility of isotopic selection of neutral species. Predissociation or fragmentation are processes which can be investigated in both time and

	Wavelength		
Experiment	**833 nm**	**820 nm**	**810 nm**
Maximization $\Re_{max}$	72	40	24.8
Minimization $\Re_{min}$	0.51	0.82	1.8
Total variation $\Re_{max}/\Re_{min}$	141	49	13.8

Table 9.7: The optimization factors obtained at different central laser wavelengths. $\Re_{max}$ is the ion ratio after maximization, $\Re_{min}$ the ion ratio after minimization between the two potassium dimer isotopes $^{39,39}K_2$ and $^{39,41}K_2$, respectively. The regular ratio under the experimental conditions in the molecular beam is $\Re_n = 6.9$.

frequency domain with the presented method on adequate molecular systems.

The large enhancement of one isotope compared to the other and vice-versa was observed at three different wavelengths (833, 820 and 810 nm). This is shown in Figure 9.28, where the major peaks present in the optimal spectra correspond to transitions between the electronic ground state $X^1\Sigma_g^+$ and the excited state $A^1\Sigma_u^+$. These transitions, associated with the first excitation step, are most significant in the isotope selection process. Moreover in some minimization experiments the isotope ratio could be reversed. Table 9.7 contains the variation factor obtained for different wavelengths by applying phase and amplitude modulation. The optimization factors decrease with decreasing wavelength. This fact is not entirely understood, but one can assume that the second excitation step, i.e. the transition $2^1\Pi_g \leftarrow A^1\Sigma_u^+$ is responsible for this decrease.

Information about the optimally chosen ionization pathway is extracted from the optimal pulse shapes, especially from their spectra. They reveal transitions which take place between particular vibrational levels of the participating electronic states.

At 833 nm a comparison between phase-only, amplitude-only and combined phase and amplitude modulation is presented, which gives hints on the involved stepwise excitation process. By comparing the results obtained for amplitude-only with combined phase and amplitude at 833 nm, it was demonstrated that information about the involved ionization path can be gained from the optimal pulse shapes. The frequency pattern play the most important role in the isotope selection process. During the first excitation step ($A^1\Sigma_u^+ \leftarrow X^1\Sigma_g^+$), a higher selectivity is achieved compared to the second excitation step ($2^1\Pi_g \leftarrow A^1\Sigma_u^+$). This displays the advantage of the applied method since different transitions can be included/excluded in the optimization by the evolutionary algorithm. From the comparison between pure phase and combined phase and amplitude modulation an insight into the molecular

dynamics could be gained as well. Since no amplitude modulation is allowed, the isotope ionization ratio can be controlled only by the time evolution of the wave packet on the electronic excited states, mainly in the $A^1\Sigma_u^+$ state with $T_{osc} = 500$ fs. This is illustrated on the multiple subpulse sequence observed in the optimal pulses. These subpulses can generated wave packets which may interfere with each other on the excited state potentials. The resulting constructive or destructive interferences may contribute to the total isotope ratio variation.

Thus the stepwise excitation at optimal frequencies followed by optimal time delays in between and the mentioned isotope-dependent constructive/destructive interference effects could lead to the high optimization factor.

In the isotope selective optimization only the ratio $\Re$ between the two potassium dimer isotopes was maximized or minimized by the shaped laser pulses. The strong amplitude modulation (considerable decrease of particular amplitudes present in the optimal pulse spectra) did not allow an enhancement of the absolute number of ions.

The femtosecond time-dependent wave packet dynamics with high spectral resolution shows the possibility of a new spectroscopical approach of sharp frequency pattern on very short time scales due to the superposition of spectral components. In the optimization experiments, where both the phase and amplitude of the femtosecond pulse were modulated, the potential of the pulse shaper was fully utilized in order to provide the necessary frequency resolution and enough freedom for the temporal evolution of the wave packets on the electronic states.

The method could be successfully applied on other model systems like potassium trimer (whereby an isotope control between $^{117}K_3$, $^{119}K_3$ or $^{121}K_3$ could be achieved) or $Na_2^{39}K$ versus $Na_2^{41}K$. These species were intensively investigated in our group in the past years. Certainly, larger molecules even with biological relevancy can be investigated and selected with this method based on the vibrational level shifts between different isotopes.